
KIMI-VL TECHNICAL REPORT

Kimi Team

ABSTRACT

We present **Kimi-VL**, an efficient open-source Mixture-of-Experts (MoE) vision-language model (VLM) that offers **advanced multimodal reasoning, long-context understanding, and strong agent capabilities**—all while activating only **2.8B** parameters in its language decoder (Kimi-VL-A3B).

Kimi-VL demonstrates strong performance across challenging domains: as a general-purpose VLM, Kimi-VL excels in multi-turn agent tasks (*e.g.*, OSWorld), matching flagship models. Furthermore, it exhibits remarkable capabilities across diverse challenging vision language tasks, including college-level image and video comprehension, OCR, mathematical reasoning, multi-image understanding. In comparative evaluations, it effectively competes with cutting-edge efficient VLMs such as GPT-4o-mini, Qwen2.5-VL-7B, and Gemma-3-12B-IT, while surpassing GPT-4o in several key domains.

Kimi-VL also advances in processing long contexts and perceiving clearly. With a 128K extended context window, Kimi-VL can process diverse long inputs, achieving impressive scores of 64.5 on LongVideoBench and 35.1 on MMLongBench-Doc. Its native-resolution vision encoder, MoonViT, further allows it to see and understand ultra-high-resolution visual inputs, achieving 83.2 on InfoVQA and 34.5 on ScreenSpot-Pro, while maintaining lower computational cost for common tasks.

Building upon Kimi-VL, we introduce an advanced long-thinking variant: **Kimi-VL-Thinking**. Developed through long chain-of-thought (CoT) supervised fine-tuning (SFT) and reinforcement learning (RL), this model exhibits strong long-horizon reasoning capabilities. It achieves scores of 61.7 on MMMU, 36.8 on MathVision, and 71.3 on MathVista while maintaining the compact 2.8B activated LLM parameters, setting a new standard for efficient yet multimodal *thinking* models. Code and models are publicly accessible at <https://github.com/MoonshotAI/Kimi-VL>.

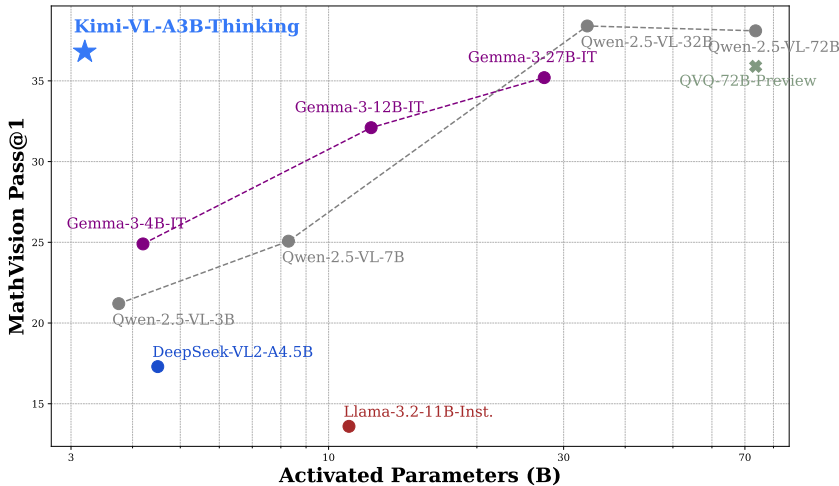


Figure 1: Comparison between **Kimi-VL-Thinking** and frontier open-source VLMs, including short-thinking VLMs (*e.g.* Gemma-3 series, Qwen2.5-VL series) and long-thinking VLMs (QVQ-72B-Preview), on MathVision benchmark. Our model achieves strong multimodal reasoning with just 2.8B LLM activated parameters.

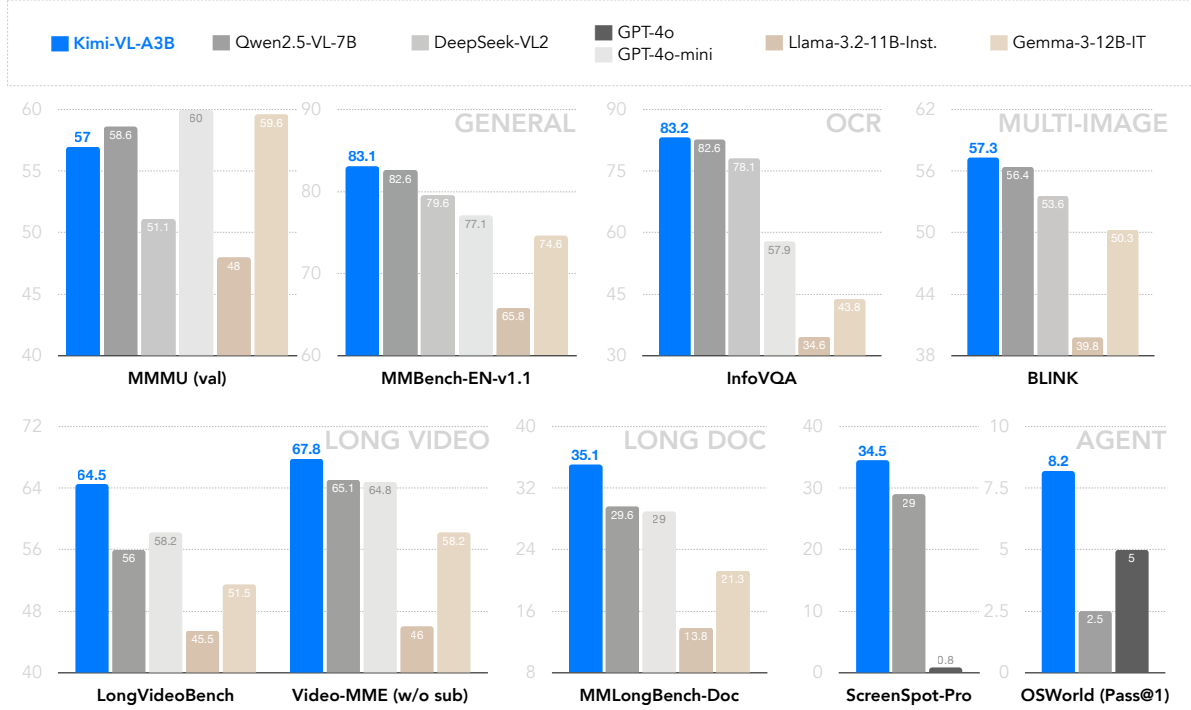


Figure 2: Highlights of **Kimi-VL** performance for a wide range of benchmarks like, general benchmarks (MMMU, MMBench), OCR (InfoVQA), multi-image (BLINK), long video (LongVideoBench, Video-MME), long document (MMLongBench-Doc), and agent (ScreenSpot-Pro and OSWorld). Detailed results are presented in Table 3.

1 Introduction

With the rapid advancement of artificial intelligence, human expectations for AI assistants have transcended traditional language-only interactions, increasingly aligning with the inherently multimodal nature of our world. To better understand and interact with these expectations, new generations of natively multimodal models, such as GPT-4o (OpenAI et al. 2024) and Google Gemini (Gemini Team et al. 2024), have emerged with the capability to seamlessly perceive and interpret visual inputs alongside language processing. Most recently, advanced multimodal models, pioneered by OpenAI o1 series (OpenAI 2024) and Kimi k1.5 (K. Team et al. 2025), have further pushed these boundaries by incorporating deeper and longer reasoning on multimodal inputs, thereby tackling more complex problems in the multimodal domain.

Nevertheless, development in large VLMs in the open-source community has significantly lagged behind their language-only counterparts, particularly in aspects of scalability, computational efficiency, and advanced reasoning capabilities. While language-only model DeepSeek R1 (DeepSeek-AI, D. Guo, et al. 2025) has already leveraged the efficient and more scalable mixture-of-experts (MoE) architecture and facilitated sophisticated long chain-of-thought (CoT) reasoning, most recent open-source VLMs, e.g. Qwen2.5-VL (Bai et al. 2025) and Gemma-3 (Gemma Team et al. 2025), continue to rely on dense architectures and do not support long-CoT reasoning. Early explorations into MoE-based vision-language models, such as DeepSeek-VL2 (Zhiyu Wu et al. 2024) and Aria (D. Li et al. 2024), exhibit limitations in other crucial dimensions. Architecturally, both models still adopt relatively traditional fixed-size vision encoders, hindering their adaptability to diverse visual inputs. From a capability perspective, DeepSeek-VL2 supports only a limited context length (4K), while Aria falls short in fine-grained visual tasks. Additionally, neither of them supports long-thinking abilities. Consequently, there remains a pressing need for an open-source VLM that effectively integrates structural innovation, stable capabilities, and enhanced reasoning through long-thinking.

In light of this, we present **Kimi-VL**, a vision-language model for the open-source community. Structurally, Kimi-VL consists of our Moonlight (J. Liu et al. 2025a) MoE language model with only **2.8B** activated (16B total) parameters, paired with a 400M native-resolution MoonViT vision encoder. In terms of capability, as illustrated in Figure 2, Kimi-VL can robustly handle diverse tasks (fine-grained perception, math, college-level problems, OCR, agent, etc.) across a broad spectrum of input forms (single-image, multi-image, video, long-document, etc.). Specifically, it features the following exciting abilities:

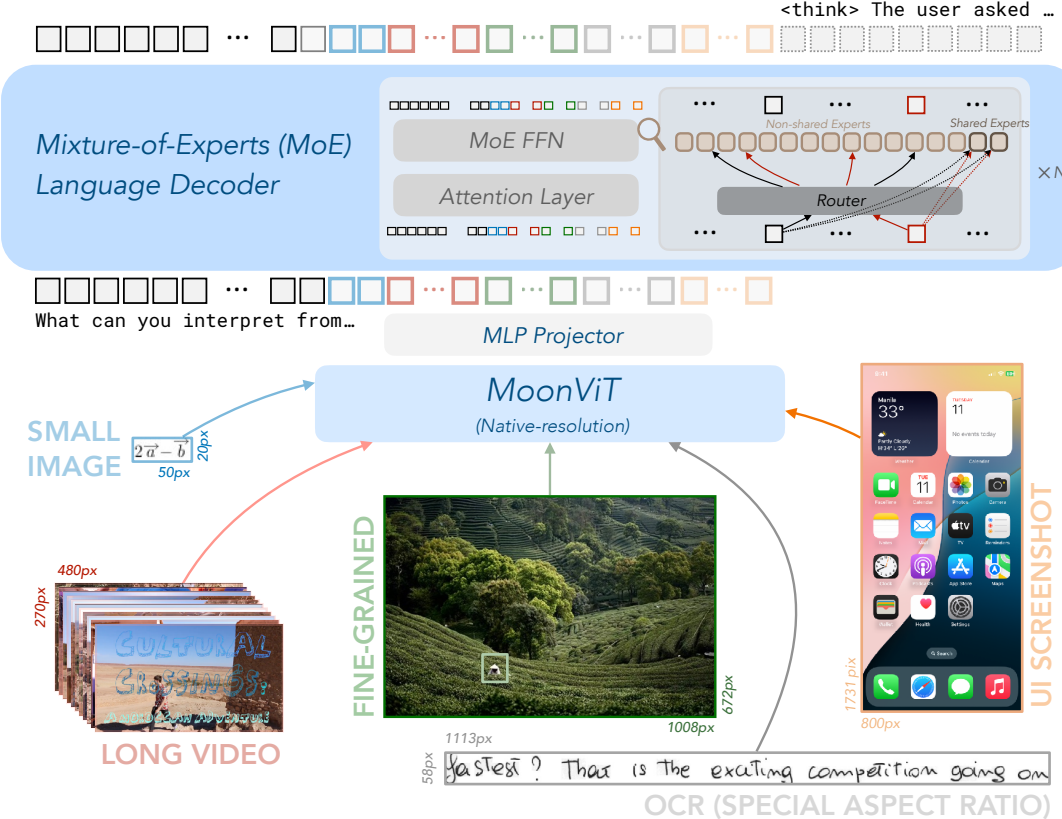


Figure 3: The model architecture of Kimi-VL and Kimi-VL-Thinking, consisting of a MoonViT that allows native-resolution images, an MLP projector, and a Mixture-of-Experts (MoE) language decoder.

- 1) **Kimi-VL is smart:** it has comparable text ability against efficient pure-text LLMs; without long thinking, Kimi-VL is already competitive in multimodal reasoning and multi-turn agent benchmarks, *e.g.*, MMMU, MathVista, OSWorld.
- 2) **Kimi-VL processes long:** it effectively tackles long-context understanding on various multimodal inputs within its 128K context window, far ahead of similar-scale competitors on long video benchmarks and MMLongBench-Doc.
- 3) **Kimi-VL perceives clear:** it shows all-round competitive ability over existing efficient dense and MoE VLMs in various vision-language scenarios: visual perception, visual world knowledge, OCR, high-resolution OS screenshot, *etc.*

Furthermore, with long-CoT activation and reinforcement learning (RL), we introduce the long-thinking version of Kimi-VL, **Kimi-VL-Thinking**, which further substantially improves performance on more complex multimodal reasoning scenarios. Despite its small scale, Kimi-VL-Thinking offers compelling performance on hard reasoning benchmarks (*e.g.*, MMMU, MathVision, MathVista), outperforming many state-of-the-art VLMs with even larger sizes.

2 Approach

2.1 Model Architecture

The architecture of Kimi-VL consists of three parts: a native-resolution vision encoder (MoonViT), an MLP projector, and an MoE language model, as depicted in Figure 3. We introduce each part in this section.

MoonViT: A Native-resolution Vision Encoder We design MoonViT, the vision encoder of Kimi-VL, to natively process images at their varying resolutions, eliminating the need for complex sub-image splitting and splicing operations, as employed in LLaVA-OneVision (B. Li et al. 2024). We incorporate the packing method from NaViT (Dehghani et al. 2023), where images are divided into patches, flattened, and sequentially concatenated into 1D sequences. These preprocessing operations enable MoonViT to share the same core computation operators and optimization as a language model, such as the variable-length sequence attention mechanism supported by FlashAttention (Dao et al. 2022), ensuring non-compromised training throughput for images of varying resolutions.



Figure 4: The pre-training stages of Kimi-VL consume a total of 4.4T tokens after text-only pre-training of its language model. To preserve text abilities, all stages that update the language model are joint training stages.

MoonViT is initialized from and continually pre-trained on SigLIP-SO-400M (Zhai et al. 2023), which originally employs learnable fixed-size absolute positional embeddings to encode spatial information. While we interpolate these original position embeddings to better preserve SigLIP’s capabilities, these interpolated embeddings become increasingly inadequate as image resolution increases. To address this limitation, we incorporate 2D rotary positional embedding (RoPE) (J. Su et al. 2023) across the height and width dimensions, which improves the representation of fine-grained positional information, especially in high-resolution images. These two positional embedding approaches work together to encode spatial information for our model and seamlessly integrate with the flattening and packing procedures. This integration enables MoonViT to efficiently process images of varying resolutions within the same batch. The resulting continuous image features are then forwarded to the MLP projector and, ultimately, to the MoE language model for subsequent training stages.

MLP Projector We employ a two-layer MLP to bridge the vision encoder (MoonViT) and the LLM. Specifically, we first use a pixel shuffle operation to compress the spatial dimension of the image features extracted by MoonViT, performing 2×2 downsampling in the spatial domain and correspondingly expanding the channel dimension. We then feed the pixel-shuffled features into a two-layer MLP to project them into the dimension of LLM embeddings.

Mixture-of-Experts (MoE) Language Model The language model of Kimi-VL utilizes our Moonlight model (J. Liu et al. 2025a), an MoE language model with 2.8B activated parameters, 16B total parameters, and an architecture similar to DeepSeek-V3 (DeepSeek-AI, A. Liu, et al. 2025). For our implementation, we initialize from an intermediate checkpoint in Moonlight’s pre-training stage—one that has processed 5.2T tokens of pure text data and activated an 8192-token (8K) context length. We then continue pre-training it using a joint recipe of multimodal and text-only data totaling 2.3T tokens, as detailed in Sec. 2.3.

2.2 Muon Optimizer

We use an enhanced Muon optimizer (J. Liu et al. 2025b) for model optimization. Compared to the original Muon optimizer (Jordan et al. 2024), we add weight decay and carefully adjust the per-parameter update scale. Additionally, we develop a distributed implementation of Muon following the ZeRO-1 (Rajbhandari et al. 2020) optimization strategy, which achieves optimal memory efficiency and reduced communication overhead while preserving the algorithm’s mathematical properties. This enhanced Muon optimizer is used throughout the entire training process to optimize all model parameters, including the vision encoder, the projector, and the language model.

2.3 Pre-Training Stages

As illustrated in Figure 4 and Table 1, after loading the intermediate language model discussed above, Kimi-VL’s pre-training comprises a total of 4 stages consuming 4.4T tokens overall: first, standalone ViT training to establish a robust native-resolution visual encoder, followed by three joint training stages (pre-training, cooldown, and long-context activation) that simultaneously enhance the model’s language and multimodal capabilities. The details are as follows.

ViT Training Stages The MoonViT is trained on image-text pairs, where the text components consist of a variety of targets: image alt texts, synthetic captions, grounding bboxes, and OCR texts. The training incorporates two objectives: a SigLIP (Zhai et al. 2023) loss \mathcal{L}_{siglip} (a variant of contrastive loss) and a cross-entropy loss $\mathcal{L}_{caption}$ for caption generation conditioned on input images. Following CoCa’s approach (J. Yu et al. 2022), the final loss function is formulated as $\mathcal{L} = \mathcal{L}_{siglip} + \lambda \mathcal{L}_{caption}$, where $\lambda = 2$. Specifically, the image and text encoders compute the contrastive loss, while the text decoder performs next-token prediction (NTP) conditioned on features from the image encoder. To accelerate training, we initialized both encoders with SigLIP SO-400M (Zhai et al. 2023) weights and implemented a progressive resolution sampling strategy to gradually allow larger size; the text decoder is initialized from a tiny decoder-only language model. During training, we observed an emergence in the caption loss while scaling up OCR

Table 1: Overview of training stages: data composition, token volumes, sequence lengths, and trainable components.

Stages	ViT Training	Joint Pre-training	JointCooldown	Joint Long-context
Data	Alt text Synthesis Caption Grounding OCR	+ Text, Knowledge Interleaving Video, Agent	+ High-quality Text High-quality Multimodal Academic Sources	+ Long Text Long Video Long Document
Tokens	2T + 0.1T	1.4T	0.6T	0.3T
Sequence length	8192	8192	8192	32768->131072
Training	ViT	ViT & LLM	ViT & LLM	ViT & LLM

Table 2: **Needle-in-a-Haystack (NIAH)** test on text/video haystacks, where needles are uniformly distributed at various positions within the haystack. We report recall accuracy across different haystack lengths up to 131,072 tokens (128K).

Haystack Length	(0, 2048]	(2048, 4096]	(4096, 8192]	(8192, 16384]	(16384, 32768]	(32768, 65536]	(65536, 131072]
- <i>text haystack</i>	100.0	100.0	100.0	100.0	100.0	100.0	87.0
- <i>video haystack</i>	100.0	100.0	100.0	100.0	100.0	100.0	91.7

data, indicating that the text decoder had developed some OCR capabilities. After training the ViT in the CoCa-alike stage with 2T tokens, we align the MoonViT to the MoE language model using another 0.1T tokens, where only MoonViT and MLP projector are updated. This alignment stage significantly reduces the initial perplexity of MoonViT embeddings in the language model, allowing a smoother joint pre-training stage as follows.

Joint Pre-training Stage In the joint pre-training stage, we train the model with a combination of pure text data (sampled from the same distribution as the initial language model) and a variety of multimodal data (as discussed in Sec. 3.1). We continue training from the loaded LLM checkpoint using the same learning rate scheduler, consuming an additional 1.4T tokens. The initial steps utilize solely language data, after which the proportion of multimodal data gradually increases. Through this progressive approach and the previous alignment stage, we observe that joint pre-training preserves the model’s language capabilities while successfully integrating visual comprehension abilities.

Joint Cooldown Stage The stage following the pre-training stage is a multimodal cooldown phase, where the model is continue trained with high-quality language and multimodal datasets to ensure superior performance. For the language part, through empirical investigation, we observe that the incorporation of synthetic data during the cooling phase yields significant performance improvements, particularly in mathematical reasoning, knowledge-based tasks, and code generation. The general text components of the cooldown dataset are curated from high-fidelity subsets of the pre-training corpus. For math, knowledge, and code domains, we employ a hybrid approach: utilizing selected pre-training subsets while augmenting them with synthetically generated content. Specifically, we leverage existing mathematical knowledge and code corpora as source material to generate question-answer (QA) pairs through a proprietary language model, implementing rejection sampling techniques to maintain quality standards (Yue, Qu, et al. 2023; D. Su et al. 2024). These synthesized QA pairs undergo comprehensive validation before being integrated into the cooldown dataset. For the multimodal part, in addition to the two strategies as employed in text cooldown data preparation, *i.e.* question-answer synthesis and high-quality subset replay, to allow more comprehensive visual-centric perception and understanding (B. Li et al. 2024; Tong et al. 2024; J. Guo et al. 2024), we filter and rewrite a variety of academic visual or vision-language data sources to QA pairs. Unlike post-training stages, these language and multimodal QA pairs in the cooldown stage are only included for activating specific abilities and henceforth facilitating learning high-quality data, thus, we keep their ratio at a low portion to avoid overfitting these QA patterns. The joint cooldown stage significantly improves both language and multimodal abilities of the model.

Joint Long-context Activation Stage In the final pre-training stage, we extend the context length of the model from 8192 (8K) to 131072 (128K), with the inverse frequency of its RoPE (J. Su et al. 2023) embeddings reset from 50,000 to 800,000. The joint long-context stage is conducted in two sub-stages, where each one extends the model’s context length by four times. For data composition, we filter and upsample the ratio of long data to 25% in each sub-stage, while using the remaining 75% tokens to replay shorter data in its previous stage; our exploration confirms that this composition allows the model to effectively learn long-context understanding while maintaining short-context ability.



Figure 5: The post-training stages of Kimi-VL and Kimi-VL-Thinking, including two stages of joint SFT in 32K and 128K context, and further long-CoT SFT and RL stages to activate and enhance long thinking abilities.

To allow the model to activate long-context abilities on both pure-text and multimodal inputs, the long data used in Kimi-VL’s long-context activation consists of not only long text, but also long multimodal data, including long interleaved data, long videos, and long documents. Similar as cooldown data, we also synthesize a small portion of QA pairs to augment the learning efficiency of long-context activation. After the long-context activations, the model can pass needle-in-a-haystack (NIAH) evaluations with either long pure-text or long video haystack, proving its versatile long-context ability. We provide the NIAH recall accuracy on various range of context length up to 128K in Table 2.

2.4 Post-Training Stages

Joint Supervised Fine-tuning (SFT) In this phase, we fine-tune the base model of Kimi-VL with instruction-based fine-tuning to enhance its ability to follow instructions and engage in dialogue, culminating in the creation of the interactive Kimi-VL model. This is achieved by employing the ChatML format (Openai, 2024), which allows for a targeted instruction optimization while maintaining architectural consistency with Kimi-VL. We optimize the language model, MLP projector, and vision encoder using a mixture of pure-text and vision-language SFT data, which will be described in Sec 3.2. Supervision is applied only to answers and special tokens, with system and user prompts being masked. The model is exposed to a curated set of multimodal instruction-response pairs, where explicit dialogue role tagging, structured injection of visual embeddings, and preservation of cross-modal positional relationships are ensured through the format-aware packing. Additionally, to guarantee the model’s comprehensive proficiency in dialogue, we incorporate a mix of multimodal data and pure text dialogue data used in Moonlight, ensuring its versatility across various dialogue scenarios.

We first train the model at the sequence length of 32k tokens for 1 epoch, followed by another epoch at the sequence length of 128k tokens. In the first stage (32K), the learning rate decays from 2×10^{-5} to 2×10^{-6} , before it re-warmups to 1×10^{-5} in the second stage (128K) and finally decays to 1×10^{-6} . To improve training efficiency, we pack multiple training examples into each single training sequence.

Long-CoT Supervised Fine-Tuning With the refined RL prompt set, we employ prompt engineering to construct a small yet high-quality long-CoT warmup dataset, containing accurately verified reasoning paths for both text and image inputs. This approach resembles rejection sampling (RS) but focuses on generating long-CoT reasoning paths through prompt engineering. The resulting warmup dataset is designed to encapsulate key cognitive processes that are fundamental to human-like reasoning, such as **planning**, where the model systematically outlines steps before execution; **evaluation**, involving critical assessment of intermediate steps; **reflection**, enabling the model to reconsider and refine its approach; and **exploration**, encouraging consideration of alternative solutions. By performing a lightweight SFT on this warm-up dataset, we effectively prime the model to internalize these multimodal reasoning strategies. As a result, the fine-tuned long-CoT model demonstrates improved capability in generating more detailed and logically coherent responses, which enhances its performance across diverse reasoning tasks.

Reinforcement Learning To further advance the model’s reasoning abilities, we then train the model with reinforcement learning (RL), enabling the model to autonomously generate structured CoT rationales. Specifically, similar as Kimi k1.5 (K. Team et al. 2025), we adopt a variant of online policy mirror descent as our RL algorithm, which iteratively refines the policy model π_θ to improve its problem-solving accuracy. During the i -th training iteration, we treat the current model as a reference policy model and optimize the following objective, regularized by relative entropy to stabilize policy updates:

$$\max_{\theta} \mathbb{E}_{(x,y^*) \sim \mathcal{D}} [\mathbb{E}_{(y,z) \sim \pi_\theta} [r(x,y,y^*)] - \tau \text{KL}(\pi_\theta(x) || \pi_{\theta_i}(x))], \quad (1)$$

where r is a reward model that justifies the correctness of the proposed answer y for the given problem x , by assigning a value $r(x,y,y^*) \in \{0, 1\}$ based on the ground truth y^* , and $\tau > 0$ is a parameter controlling the degree of regularization.

Each training iteration begins by sampling a problem batch from the dataset \mathcal{D} , and the model parameters are updated to θ_{i+1} using the policy gradient derived from (1), with the optimized policy model subsequently assuming the role of reference policy for the subsequent iteration. To enhance RL training efficiency, we implement a length-based reward to penalize excessively long responses, mitigating the overthinking problem where the model generates redundant reasoning chains. Besides, we employ two sampling strategies including curriculum sampling and prioritized sampling, which leverage difficulty labels and per-instance success rates to focus training effort on the most pedagogically valuable examples, thereby optimizing the learning trajectory and improving training efficiency.

Through large-scale reinforcement learning training, we can derive a model that harnesses the strengths of both basic prompt-based CoT reasoning and sophisticated planning-enhanced CoT approaches. During inference, the model maintains standard autoregressive sequence generation, eliminating the deployment complexities associated with specialized planning algorithms that require parallel computation. Simultaneously, the model develops essential meta-reasoning abilities including error detection, backtracking, and iterative solution refinement by effectively utilizing the complete history of explored reasoning paths as contextual information. With endogenous learning from its complete reasoning trace history, the model can effectively encode planned search procedures into its parametric knowledge.

2.5 Infrastructure

Storage We utilize S3 (Amazon Web Services 2023) compatible object storage from cloud service vendors to store our visual-text data. To minimize the time between data preparation and model training, we store visual data in its original format and have developed an efficient and flexible data loading system. This system provides several key benefits:

- Supports on-the-fly data shuffling, mixing, tokenization, loss masking and packing during training, allowing us to adjust data proportions as needed;
- Enables random augmentation of both visual and text data, while preserving the correctness of 2D coordinate and orientation information during transformations;
- Ensures reproducibility by strictly controlling random states and other states across different data loader workers, guaranteeing that any interrupted training can be resumed seamlessly—the data sequence after resumption remains identical to an uninterrupted run;
- Delivers high-performance data loading; through multiple caching strategies, our system reliably supports training on large scale clusters while maintaining controlled request rates and throughput to the object storage.

Additionally, to ensure consistent dataset quality control, we developed a centralized platform for data registration, visualization, compiling statistics, synchronizing data across cloud storage systems, and managing dataset lifecycles.

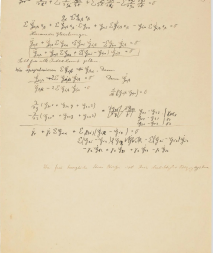
Parallelism We adopt a 4D parallelism strategy—Data Parallelism (S. Li et al. 2020), Expert Parallelism (Fedus et al. 2022), Pipeline Parallelism (Y. Huang et al. 2019; Narayanan et al. 2021), and Context Parallelism (Jacobs et al. 2023; H. Liu et al. 2023)—to accelerate the speed of Kimi-VL . After optimizing parallel strategies, the resulting training throughput of our model is around 60% higher than a 7B dense VLM (*e.g.* VLMs based on Qwen2.5-7B).

- **Data Parallelism (DP).** DP replicates the model across multiple devices, each processing different micro-batches. This setup allows larger effective batch sizes by simply increasing the number of devices.
- **Expert Parallelism (EP).** EP distributes expert modules in the MoE layer across multiple devices. When combined with DP, experts on a given device can handle tokens from different DP groups, enhancing computational efficiency.
- **Pipeline Parallelism (PP).** PP splits the model into multiple layer-based stages. To minimize pipeline bubbles, we allocate the Vision Tower (VT) and several decoder layers to the first stage, place the output layer and additional decoder layers in the last stage, and distribute the remaining decoder layers evenly across intermediate stages based on their time overhead.
- **Context Parallelism (CP).** CP addresses long-sequence training by splitting sequences across different CP ranks in conjunction with flash attention (Dao et al. 2022). This substantially reduces peak memory usage and relieves the memory pressure from attention computations.

Beyond these four parallel strategies, we incorporate ZeRO1 (Rajbhandari et al. 2020) and Selective Checkpointing Activation (T. Chen et al. 2016; Korthikanti et al. 2022) to further optimize memory usage. ZeRO1 reduces optimizer state overhead by using a distributed optimizer while avoiding extra communication costs. Selective Checkpointing Activation trades time for space by recomputing only those layers that have low time overhead but high memory consumption, striking a balance between computation efficiency and memory demands. For extremely long sequences, we expand recomputation to a broader set of layers to prevent out-of-memory errors.

Instruction

Please infer step by step who this manuscript belongs to and what it records



Response

<Think> Alright, I need to figure out who this manuscript belongs to and what it records based on the images provided. Let's start by analyzing the images carefully.

First, I'll look at the visual characteristics of the manuscript. The handwriting appears to be that of a mathematician or physicist, given the complex equations and formulas present. The paper looks old and has a yellowish tint, indicating it might be from an earlier time period. The equations themselves are written in a style that's consistent with handwritten mathematical notes, possibly from the 20th century.

Next, I'll examine the content of the manuscripts. Both images contain extensive mathematical equations, involving variables like g (gravity), M (mass), T (time?), and various indices and summations. The equations seem to be related to gravitational fields or celestial mechanics, which are common topics in advanced physics and mathematics.

Looking at the first image (Image 1), I can see equations involving partial derivatives and summations, which are typical in field theory or tensor calculus. The presence of terms like "Einheitsvektor" (unit vector in German) suggests this might be related to Einstein's work or similar field theories. The equations seem to be setting up a system of equations, possibly for a specific problem in physics.

The second image (Image 2) contains more numerical calculations and formulas. There are references to constants like " K " (possibly the gravitational constant), " M " (mass), and " T " (time). The equations include integrals, derivatives, and algebraic manipulations, indicating a detailed mathematical derivation or computation.

Now, considering the writing style and the content, I notice that the handwriting is somewhat messy but consistent, suggesting it's from a single author. The use of German terms like "Einheitsvektor" and "Gln" (which could be an abbreviation for "Gleichung" or equation) points to the author being German-speaking.

The first image seems to be a page from a mathematical manuscript, possibly from Einstein's work, given the style and content. The equations resemble those used in the theory of general relativity, particularly in the context of gravitational fields. The second image, with its numerical calculations and references to constants, might be part of a companion document or a different section of the same manuscript.

Putting this together, the manuscripts likely belong to Albert Einstein, given the style of the equations and the content related to gravitational fields and field theory. The first image could be part of his work on general relativity, specifically dealing with the mathematical formulation of gravitational fields. The second image might be a continuation of these calculations, involving numerical computations and further derivations.

To verify, I'll consider the following points:

1. The presence of German terms suggests a German-speaking author, which aligns with Einstein's background.
2. The complex mathematical content matches Einstein's known work in field theory and general relativity.
3. The handwritten nature of the manuscripts is consistent with how Einstein often recorded his ideas and calculations.

Given these observations, I conclude that the manuscripts belong to Albert Einstein and record his work on gravitational field equations and related mathematical derivations, possibly from his research on general relativity or a related field in physics.</Think>

The manuscripts in the images belong to **Albert Einstein**, a renowned physicist known for his contributions to the theory of general relativity. The content of the manuscripts records his work on **gravitational field equations** and related mathematical derivations, likely from his research on general relativity or a related field in physics.

Key Observations:

1. **Handwriting Style:** The handwriting is consistent with Einstein's known style, characterized by careful, albeit slightly messy, mathematical notation.
2. **Content Analysis:**
 - The equations involve terms like **partial derivatives**, **summations**, and **Greek letters** (e.g., α , β , γ), which are typical in tensor calculus and field theory.
 - The first image shows equations that resemble **Einstein's formulation** of gravitational field equations, possibly related to the Einstein field equations in general relativity.
 - The second image includes numerical calculations, constants (e.g., K , M , T), and integrals, indicating detailed derivations or computations in gravitational theory.
3. **German Terms:** The presence of German terms like "Einheitsvektor" (unit vector) and "Gln" (equation) suggests Einstein, who was German-speaking.

Conclusion:

These manuscripts are part of Einstein's research materials, documenting his mathematical and theoretical work on gravitational fields and field equations. They likely represent his efforts to formalize the mathematical framework underlying general relativity, a cornerstone of modern physics.

Final Answer:

The manuscripts belong to Albert Einstein and record his work on gravitational field equations and mathematical derivations in general relativity.

Figure 6: Manuscript reasoning visualization. Kimi-VL-Thinking demonstrates the ability to perform historical and scientific inference by analyzing handwritten manuscripts step by step. In this example, our model identifies the author as Albert Einstein based on handwriting style, content analysis, and language cues. It reasons that the manuscripts relate to gravitational field equations, consistent with Einstein's contributions to general relativity.

3 Data Construction

3.1 Pre-Training Data

Our multimodal pre-training corpus is designed to provide high-quality data that enables models to process and understand information from multiple modalities, including text, images, and videos. To this end, we have also curated high-quality data from six categories – caption, interleaving, OCR, knowledge, video, and agent – to form the corpus.

When constructing our training corpus, we developed several multimodal data processing pipelines to ensure data quality, encompassing filtering, synthesis, and deduplication. Establishing an effective multimodal data strategy is crucial during the joint training of vision and language, as it both preserves the capabilities of the language model and facilitates alignment of knowledge across diverse modalities.

We provide a detailed description of these sources in this section, which is organized into the following categories:

Caption Data Our caption data provides the model with fundamental modality alignment and a broad range of world knowledge. By incorporating caption data, the multimodal LLM gains wider world knowledge with high learning efficiency. We have integrated various open-source Chinese and English caption datasets like (Schuhmann et al. 2022; Gadre et al. 2024) and also collected substantial in-house caption data from multiple sources. However, throughout the training process, we strictly limit the proportion of synthetic caption data to mitigate the risk of hallucination stemming from insufficient real-world knowledge.

For general caption data, we follow a rigorous quality control pipeline that avoids duplication and maintain high image-text correlation. We also vary image resolution during pre-training to ensure that the vision tower remains effective when processing images of both high- and low-resolution.

Image-text Interleaving Data During the pre-training phase, the model benefits from interleaving data for many aspects. For example, multi-image comprehension ability can be boosted by interleaving data; interleaving data always provides detailed knowledge for the given image; a longer multimodal context learning ability can also be gained by interleaving data. What's more, we also find that interleaving data can contribute positively to maintaining the model's

8

language abilities. Thus, image-text interleaving data is an important part in our training corpus. Our multimodal corpus considered open-sourced interleave datasets like (Zhu et al. 2024; Laurençon et al. 2024) and also constructed large-scale in-house data using resources like textbooks, webpages, and tutorials. Further, we also find that synthesizing the interleaving data benefits the performance of multimodal LLM for keeping the text knowledge. To ensure each image’s knowledge is sufficiently studied, for all the interleaving data, despite standard filtering, deduping, and other quality control pipeline, we also integrate a data reordering procedure to keep all the image and text in the correct order.

OCR Data Optical Character Recognition (OCR) is a widely adopted technique that converts text from images into an editable format. In our model, a robust OCR capability is deemed essential for better aligning the model with human values. Accordingly, our OCR data sources are diverse, ranging from open-source to in-house datasets, encompassing both clean and augmented images, and spanning over single-page and multi-page inputs.

In addition to the publicly available data, we have developed a substantial volume of in-house OCR datasets, covering multilingual text, dense text layouts, web-based content, and handwritten samples. Furthermore, following the principles outlined in OCR 2.0 (Wei et al. 2024), our model is also equipped to handle a variety of optical image types, including figures, tables, geometry diagrams, mermaid plots, and natural scene text. We apply extensive data augmentation techniques—such as rotation, distortion, color adjustments, and noise addition—to enhance the model’s robustness. As a result, our model achieves a high level of proficiency in OCR tasks.

In addition to single-page OCR data, we collect and convert a large volume of in-house multi-page OCR data to activate the model’s understanding of long documents in the real world. With the help of these data, our model is capable of performing accurate OCR on a single image but can also comprehend an entire academic paper or a scanned book.

Knowledge Data The concept of multimodal knowledge data is analogous to the previously mentioned text pre-training data, except here we focus on assembling a comprehensive repository of human knowledge from diverse sources to further enhance the model’s capabilities. For example, carefully curated geometry data in our dataset is vital for developing visual reasoning skills, ensuring the model can interpret the abstract diagrams created by humans.

Our knowledge corpus adheres to a standardized taxonomy to balance content across various categories, ensuring diversity in data sources. Similar to text-only corpora, which gather knowledge from textbooks, research papers, and other academic materials, multimodal knowledge data employs both a layout parser and an OCR model to process content from these sources. While we also include filtered data from internet-based and other external resources.

Because a significant portion of our knowledge corpus is sourced from internet-based materials, infographics can cause the model to focus solely on OCR-based information. In such cases, relying exclusively on a basic OCR pipeline may limit training effectiveness. To address this, we have developed an additional pipeline that better captures the purely textual information embedded within images.

Agent Data For agent tasks, the model’s grounding and planning capabilities have been significantly enhanced. In addition to utilizing publicly available data, a platform has been established to efficiently manage and execute virtual machine environments in bulk. Within these virtual environments, heuristic methods were employed to collect screenshots and corresponding action data. This data was then processed into dense grounding formats and continuous trajectory formats. The design of the Action Space was categorized according to Desktop, Mobile, and Web environments. Furthermore, icon data was collected to strengthen the model’s understanding of the meanings of icons within software graphical user interfaces (GUIs). To enhance the model’s planning ability for solving multi-step desktop tasks, a set of computer-use trajectories was collected from human annotators, each accompanied by synthesized Chain-of-Thought (Aguvis ??). These multi-step agent demonstrations equip Kimi-Flash with the capability to complete real-world desktop tasks (on both Ubuntu and Windows).

Video Data In addition to image-only and image-text interleaved data, we also incorporate large-scale video data during pre-training, cooldown, and long-context activation stages to enable two directions of essential abilities of our model: first, to understand a long-context sequence dominated by images (*e.g.* hour-long videos) in addition to long text; second, to perceive fine-grained spatio-temporal correspondence in short video clips.

Our video data are sourced from diverse resources, including open-source datasets as well as in-house web-scale video data, and span videos of varying durations. Similarly, to ensure sufficient generalization ability, our video data cover a wide range of scenes and diverse tasks. We cover tasks such as video description and video grounding, among others. For long videos, we carefully design a pipeline to produce dense captions. Similar to processing the caption data, we strictly limit the proportion of the synthetic dense video description data to reduce the risk of hallucinations.

Text Data Our text pretrain corpus directly utilizes the data in Moonlight J. Liu et al. 2025a, which is designed to provide comprehensive and high-quality data for training large language models (LLMs). It encompasses five domains: English, Chinese, Code, Mathematics & Reasoning, and Knowledge. We employ sophisticated filtering and quality control mechanisms for each domain to ensure the highest quality training data. For all pretrain data, we conducted

rigorous individual validation for each data source to assess its specific contribution to the overall training recipe. This systematic evaluation ensures the quality and effectiveness of our diverse data composition. To optimize the overall composition of our training corpus, the sampling strategy for different document types is empirically determined through extensive experimentation. We conduct isolated evaluations to identify document subsets that contribute most significantly to the model’s knowledge acquisition capabilities. These high-value subsets are upsampled in the final training corpus. However, to maintain data diversity and ensure model generalization, we carefully preserve a balanced representation of other document types at appropriate ratios. This data-driven approach helps us optimize the trade-off between focused knowledge acquisition and broad generalization capabilities.

Benchmark (Metric)	GPT-4o	GPT-4o-mini	Qwen2.5- VL-7B	Llama3.2- 11B-Inst.	Gemma3- 12B-IT	DeepSeek- VL2	Kimi-VL- A3B	
Architecture	-	-	Dense	Dense	Dense	MoE	MoE	
	-	-	7.6B+0.7B	8B+2.6B	12B+0.4B	4.1B+0.4B	2.8B+0.4B	
	-	-	8B	11B	12B	28B	16B	
College-level	MMMU _{val} (Pass@1)	69.1	60.0	58.6	48	<u>59.6</u>	51.1	57.0
	VideoMMMU (Pass@1)	61.2	-	47.4	41.8	57.2	44.4	<u>52.6</u>
	MMVU _{val} (Pass@1)	67.4	61.6	50.1	44.4	<u>57.0</u>	52.1	52.2
General	MMBench-EN-v1.1 (Acc)	83.1	77.1	<u>82.6</u>	65.8	74.6	79.6	83.1
	MMStar (Acc)	64.7	54.8	63.9	49.8	56.1	55.5	<u>61.3</u>
	MMVet (Pass@1)	69.1	<u>66.9</u>	67.1	57.6	64.9	60.0	66.7
	RealWorldQA (Acc)	75.4	67.1	68.5	63.3	59.1	<u>68.4</u>	68.1
	AI2D (Acc)	84.6	77.8	<u>83.9</u>	77.3	78.1	81.4	84.9
Multi-image	BLINK (Acc)	68.0	53.6	<u>56.4</u>	39.8	50.3	-	57.3
Math	MathVista (Pass@1)	63.8	52.5	<u>68.2</u>	47.7	56.1	62.8	68.7
	MathVision (Pass@1)	30.4	-	<u>25.1</u>	13.6	32.1	17.3	21.4
OCR	InfoVQA (Acc)	80.7	57.9	<u>82.6</u>	34.6	43.8	78.1	83.2
	OCRBench (Acc)	815	785	<u>864</u>	753	702	811	867
OS Agent	ScreenSpot-V2 (Acc)	18.1	-	<u>86.8</u>	-	-	-	92.8
	ScreenSpot-Pro (Acc)	0.8	-	<u>29.0</u>	-	-	-	34.5
	OSWorld (Pass@1)	5.03	-	<u>2.5</u>	-	-	-	8.22
	WindowsAgentArena (Pass@1)*	9.4	2.7	<u>3.4</u>	-	-	-	10.4
Long Document	MMLongBench-Doc (Acc)	42.8	29.0	<u>29.6</u>	13.8	21.3	-	35.1
Long Video	Video-MME (w/o sub. / w/ sub.)	71.9/77.2	64.8/68.9	<u>65.1/71.6</u>	46.0/49.5	58.2/62.1	-	67.8/72.6
	MLVU _{MCQ} (Acc)	64.6	48.1	<u>70.2</u>	44.4	52.3	-	74.2
	LongVideoBench _{val}	66.7	<u>58.2</u>	56.0	45.5	51.5	-	64.5
Video Perception	EgoSchema _{full}	72.2	-	<u>65.0</u>	54.3	56.9	38.5	78.5
	VSI-Bench	34.0	-	<u>34.2</u>	20.6	32.4	21.7	37.4
	TOMATO	37.7	<u>28.8</u>	27.6	21.5	28.6	27.2	31.7

Table 3: Performance of Kimi-VL against proprietary and open-source efficient VLMs; performance of GPT-4o is also listed in gray for reference. Top and second-best models are in **boldface** and underline respectively. Some results of competing models are unavailable due to limitation of model ability on specific tasks or model context length.

*GPT-4o and GPT-4o-mini results use Omniparser without UIA, according to Bonatti et al. 2024.

 **Instruction**

Which of the four subgraphs in the figure is taken at the same place as subgraph 1?



 **Response**

The first picture (image 1) depicts a dense urban area with a mix of buildings, green spaces, and a distinctive circular structure (possibly a dome or observatory). To determine which sub-picture matches this location:

Image 4 shows a similarly dense urban environment with a large building complex featuring a central courtyard and a circular structure resembling the one in image 1. Both images share the same type of urban layout, building density, and green spaces. Image 3 includes a church spire (not present in image 1) and a more spread-out layout, making it distinct.

Image 2 is clearly suburban with larger plots and fewer buildings, unlike the compact urban setting of image 1.

Conclusion: Image 4 is the most likely candidate as it matches the urban density, building types, and the circular structure seen in image 1.

Answer: The fourth sub-picture (image 4) is in the same place as the first picture.

 **Instruction**

What is the dome building in the picture?



 **Response**

The dome building in the image is the Rogers Centre, a multi-purpose stadium in Toronto, Canada. It is recognizable by its distinctive retractable roof and is a landmark in the city's skyline, often visible alongside the CN Tower (the tall spire in the background). The Rogers Centre hosts various events, including sports games, concerts, and conventions.

 **Instruction**

Where am I ?



 **Response**

You are in Cyberpunk 2077, an open-world action role-playing game set in Night City (year 2077). The image shows a futuristic bar or club within the game's cyberpunk-themed environment, likely a mission or social interaction location (e.g., "Sit next to Jackie" is visible in the HUD). The setting features neon lights, holographic displays, and characters with cybernetic enhancements, typical of the game's aesthetic.

Figure 7: Kimi-VL exhibits strong visual reasoning capabilities by grounding visual content in spatial, contextual, and cultural knowledge. It accurately identifies matching urban locations based on structural and layout features, interprets scenes from video games like Cyberpunk 2077 using stylistic cues, and recognizes real-world landmarks such as the Rogers Centre in Toronto.

3.2 Instruction Data

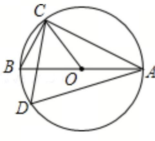
At this stage, the data is primarily aimed at enhancing the model’s conversational abilities and instruction-following capabilities. To cover as many scenarios as possible, we enrich the data across different domains. For non-reasoning tasks, including chart interpretation, agent grounding, OCR, image-grounded conversations, question-answering, writing, and text processing, we initially construct a seed dataset through human annotation. This seed dataset is used to train a seed model. Subsequently, we collect a diverse set of prompts and employ the seed model to generate multiple responses to each prompt. Annotators then rank these responses and refine the top-ranked response to produce the final version. For reasoning tasks like visual coding, visual reasoning, and math/science problems, where rule-based and model-based verifications are more accurate and efficient than human judgment, we utilize rejection sampling to expand the SFT dataset. The complete vanilla SFT dataset comprises approximately a 1:1 ratio of text tokens to image tokens.

3.3 Reasoning Data

Our reasoning data is meticulously constructed for activation and enhancement of the model’s multimodal reasoning capabilities during both the long-CoT supervised fine-tuning and reinforcement learning stages. Through developing a generation pipeline that resembles rejection sampling (RS) and prompt engineering, we collect and synthesize an amount of high-quality long-CoT data. Specifically, we first assemble a collection of QA data with ground truth annotations that require multi-step reasoning, such as mathematical problem-solving and domain-specific VQA. Subsequently, we sample multiple detailed reasoning trajectories for each question by leveraging a powerful long-CoT model -

 **Instruction**

回答问题



如图,AB为 $\odot O$ 的直径,点D、C在 $\odot O$ 上, $\angle D=62^\circ$,则 $\angle ACO$ 的度数为() A. 26° B. 28° C. 30° D. 32°

 **Response**

根据题目描述, AB是圆O的直径, 点D和C在圆O上, 且 $\angle D = 62^\circ$ 。我们需要求 $\angle ACO$ 的度数。

1. 分析已知条件:

- AB是直径, 所以 $\angle ACB = 90^\circ$ (圆周角定理)。
- $\angle D = 62^\circ$ 。

2. 利用圆周角定理:

- $\angle AOC$ 是圆心角, 等于2倍的圆周角 $\angle D$ 。
- $\angle AOC = 2 \times 62^\circ = 124^\circ$ 。

3. 计算 $\angle ACO$:

- $\angle ACO$ 是三角形AOC的内角。
- $\angle ACO + \angle CAO + \angle AOC = 180^\circ$ 。
- 因为OA = OC (半径相等), 所以 $\angle CAO = \angle ACO$ 。
- 设 $\angle ACO = x$, 则:

$$\begin{aligned} x + x + 124^\circ &= 180^\circ \\ 2x + 124^\circ &= 180^\circ \\ 2x &= 56^\circ \\ x &= 28^\circ \end{aligned}$$

因此, $\angle ACO$ 的度数为 28° 。答案是B。

Figure 8: Kimi-VL demonstrates its capability to perform symbolic reasoning and geometric inference by solving a circle geometry problem step by step. The model analyzes given conditions, applies geometric theorems such as the inscribed angle theorem and properties of triangle angles, and accurately derives the target angle.

Kimi k1.5 (K. Team et al. 2025) with curated reasoning prompts. In rejection sampling, we feed the true labels and model predictions into an off-the-shelf reward model for judgment. Wrong chain-of-thought responses are filtered out according to the model evaluation as well as some rule-based rewards, thus improving the reasoning data quality.

4 Evaluation

We begin by presenting our comprehensive model and conducting a comparative analysis with leading state-of-the-art (SoTA) solutions. Following this introduction, we proceed to assess various sub-capabilities of the model through detailed performance evaluations. This part examines how effectively the model handles different tasks and scenarios, providing insights into its strengths and limitations across diverse functional domains.

4.1 Comparison to the State-of-the-Art Models

Table 3 presents a comprehensive evaluation of Kimi-VL against state-of-the-art vision-language models across multiple benchmarks. Although having a more parameter-efficient architecture (2.8B+0.4B activated parameters) compared to larger models such as GPT-4o, Llama-3.2-11B-Inst. and Gemma3-12B-IT, Kimi-VL demonstrates competitive or superior performance in several key areas. Our model employs a Mixture-of-Experts (MoE) architecture similar to DeepSeek-VL2, but outperforms it on most benchmarks with significantly fewer parameters (activated: 2.8B vs 4.5B; total: 16B vs 28B); it also outperforms Qwen2.5-VL-7B (*actually 8.3B*) on 19 out of 24 benchmarks, though the latter has 2.59× more activated parameters. The following sections analyze performance across specific domains, which reveals Kimi-VL's strengths in OCR, math, agent, long-form content understanding, multi-image and video perception.

4.1.1 College-level Academic Problems

Our Kimi-VL model demonstrates competitive performance on college-level academic benchmarks. On MMMU validation set, it achieves a score of 57.0%, which outperforms DeepSeek-VL2 (51.1%) and is comparable to Qwen2.5-

Instruction

Parse the complete table and output it in markdown table format.

Sparkling Smiles Clinic Rate Analysis		2014	2015	2016	2017	2018	2019	2020	2021
Growth	Yearly Growth	-5%	5%	-7%	7%	-7%	7%	-7%	7%
Patient Total Assets		2014	2015	2016	2017	2018	2019	2020	2021
Current Assets		175	175	175	175	175	175	175	175
Long-term Assets		175	175	175	175	175	175	175	175
Total Assets		350	350	350	350	350	350	350	350
Patient Current Liabilities		150	150	150	150	150	150	150	150
Long-term Liabilities		150	150	150	150	150	150	150	150
Total Liabilities		300	300	300	300	300	300	300	300
Patient Net Assets		50	50	50	50	50	50	50	50
Gross Profit		125	125	125	125	125	125	125	125
Selling, General & Administrative Expenses		75	75	75	75	75	75	75	75
Profit Before Interest and Taxes		50	50	50	50	50	50	50	50
Net Income		40	40	40	40	40	40	40	40
Dividends		10	10	10	10	10	10	10	10
Total Net Income		30	30	30	30	30	30	30	30
Total Assets		350	350	350	350	350	350	350	350
Total Liabilities		300	300	300	300	300	300	300	300
Current Assets		175	175	175	175	175	175	175	175
Long-term Assets		175	175	175	175	175	175	175	175
Total Assets		350	350	350	350	350	350	350	350
Current Liabilities		150	150	150	150	150	150	150	150
Long-term Liabilities		150	150	150	150	150	150	150	150
Total Liabilities		300	300	300	300	300	300	300	300
Patient Net Assets		50	50	50	50	50	50	50	50
Gross Profit Margin		35%	35%	35%	35%	35%	35%	35%	35%
Net Profit Margin		20%	20%	20%	20%	20%	20%	20%	20%
Activity Period		2014	2015	2016	2017	2018	2019	2020	2021
Operating Duration		75.21	81.14	87.07	93.00	98.93	104.86	110.79	116.72

Instruction

Please generate the latex code of the formula in the image.

$$\mathbf{x}_{t-1} \sim q(\mathbf{x}_{t-1} | \mathbf{x}_t, \mathbf{z}_0) = \mathcal{N}(\boldsymbol{\mu}_q, \boldsymbol{\Sigma}_q) = \mathcal{N}\left(\frac{\sqrt{\alpha_t}(1-\bar{\alpha}_{t-1})\mathbf{x}_t + \sqrt{\bar{\alpha}_{t-1}}(1-\alpha_t)\mathbf{z}_0}{1-\bar{\alpha}_t}, \frac{(1-\alpha_t)(1-\bar{\alpha}_{t-1})}{1-\bar{\alpha}_t} \mathbf{I}\right)$$

$$= \mathcal{N}\left(\frac{\sqrt{\bar{\alpha}_{t-1}}\beta_t}{1-\bar{\alpha}_t} \mathbf{x}_0 + \frac{\sqrt{\alpha_t}(1-\bar{\alpha}_{t-1})}{1-\bar{\alpha}_t} \mathbf{x}_t, \frac{1-\bar{\alpha}_{t-1}}{1-\bar{\alpha}_t} \beta_t \mathbf{I}\right)$$

Response

```
#< Sparkling Smiles Clinic - Profit Analysis
## Growth
# Yearly Sales Growth
|-----|-----|-----|-----|-----|-----|-----|-----|-----|
| 2014 | 1.25% | 1.25% | 1.25% | 1.25% | 1.25% | 1.25% | 1.25% | 1.25% |
| 2015 | 1.25% | 1.25% | 1.25% | 1.25% | 1.25% | 1.25% | 1.25% | 1.25% |
| 2016 | 1.25% | 1.25% | 1.25% | 1.25% | 1.25% | 1.25% | 1.25% | 1.25% |
| 2017 | 1.25% | 1.25% | 1.25% | 1.25% | 1.25% | 1.25% | 1.25% | 1.25% |
| 2018 | 1.25% | 1.25% | 1.25% | 1.25% | 1.25% | 1.25% | 1.25% | 1.25% |
| 2019 | 1.25% | 1.25% | 1.25% | 1.25% | 1.25% | 1.25% | 1.25% | 1.25% |
| 2020 | 1.25% | 1.25% | 1.25% | 1.25% | 1.25% | 1.25% | 1.25% | 1.25% |
| 2021 | 1.25% | 1.25% | 1.25% | 1.25% | 1.25% | 1.25% | 1.25% | 1.25% |
|-----|-----|-----|-----|-----|-----|-----|-----|-----|
## Percent of Total Assets
# Year: Inventory / Other Current Assets / Total Current Assets / Long-term Assets / Total Assets / Current Liabilities
|-----|-----|-----|-----|-----|-----|-----|-----|-----|
| 2014 | 100% | 100% | 100% | 100% | 100% | 100% | 100% | 100% |
| 2015 | 100% | 100% | 100% | 100% | 100% | 100% | 100% | 100% |
| 2016 | 100% | 100% | 100% | 100% | 100% | 100% | 100% | 100% |
| 2017 | 100% | 100% | 100% | 100% | 100% | 100% | 100% | 100% |
| 2018 | 100% | 100% | 100% | 100% | 100% | 100% | 100% | 100% |
| 2019 | 100% | 100% | 100% | 100% | 100% | 100% | 100% | 100% |
| 2020 | 100% | 100% | 100% | 100% | 100% | 100% | 100% | 100% |
| 2021 | 100% | 100% | 100% | 100% | 100% | 100% | 100% | 100% |
|-----|-----|-----|-----|-----|-----|-----|-----|-----|
## Percent of Total Assets
# Year: Inventory / Other Current Assets / Total Current Assets / Long-term Assets / Total Assets / Current Liabilities
|-----|-----|-----|-----|-----|-----|-----|-----|-----|
| 2014 | 100% | 100% | 100% | 100% | 100% | 100% | 100% | 100% |
| 2015 | 100% | 100% | 100% | 100% | 100% | 100% | 100% | 100% |
| 2016 | 100% | 100% | 100% | 100% | 100% | 100% | 100% | 100% |
| 2017 | 100% | 100% | 100% | 100% | 100% | 100% | 100% | 100% |
| 2018 | 100% | 100% | 100% | 100% | 100% | 100% | 100% | 100% |
| 2019 | 100% | 100% | 100% | 100% | 100% | 100% | 100% | 100% |
| 2020 | 100% | 100% | 100% | 100% | 100% | 100% | 100% | 100% |
| 2021 | 100% | 100% | 100% | 100% | 100% | 100% | 100% | 100% |
|-----|-----|-----|-----|-----|-----|-----|-----|-----|
## Percent of Sales
# Year: Sales / Selling, General & Administrative Expenses / Advertising Expenses / Profit Before Interest and Taxes
|-----|-----|-----|-----|-----|-----|-----|-----|-----|
| 2014 | 1.25% | 1.25% | 1.25% | 1.25% | 1.25% | 1.25% | 1.25% | 1.25% |
| 2015 | 1.25% | 1.25% | 1.25% | 1.25% | 1.25% | 1.25% | 1.25% | 1.25% |
| 2016 | 1.25% | 1.25% | 1.25% | 1.25% | 1.25% | 1.25% | 1.25% | 1.25% |
| 2017 | 1.25% | 1.25% | 1.25% | 1.25% | 1.25% | 1.25% | 1.25% | 1.25% |
| 2018 | 1.25% | 1.25% | 1.25% | 1.25% | 1.25% | 1.25% | 1.25% | 1.25% |
| 2019 | 1.25% | 1.25% | 1.25% | 1.25% | 1.25% | 1.25% | 1.25% | 1.25% |
| 2020 | 1.25% | 1.25% | 1.25% | 1.25% | 1.25% | 1.25% | 1.25% | 1.25% |
| 2021 | 1.25% | 1.25% | 1.25% | 1.25% | 1.25% | 1.25% | 1.25% | 1.25% |
|-----|-----|-----|-----|-----|-----|-----|-----|-----|
## Math Ratios
# Year: Net Profit Margin / Quick Ratio / Total Debt to Total Assets / Pre-tax Return on Net Worth / Pre-tax Return on Assets
|-----|-----|-----|-----|-----|-----|-----|-----|-----|
| 2014 | 0.40% | 0.40% | 1.25% | 1.25% | 1.25% | 1.25% | 1.25% | 1.25% |
| 2015 | 0.40% | 0.40% | 1.25% | 1.25% | 1.25% | 1.25% | 1.25% | 1.25% |
| 2016 | 0.40% | 0.40% | 1.25% | 1.25% | 1.25% | 1.25% | 1.25% | 1.25% |
| 2017 | 0.40% | 0.40% | 1.25% | 1.25% | 1.25% | 1.25% | 1.25% | 1.25% |
| 2018 | 0.40% | 0.40% | 1.25% | 1.25% | 1.25% | 1.25% | 1.25% | 1.25% |
| 2019 | 0.40% | 0.40% | 1.25% | 1.25% | 1.25% | 1.25% | 1.25% | 1.25% |
| 2020 | 0.40% | 0.40% | 1.25% | 1.25% | 1.25% | 1.25% | 1.25% | 1.25% |
| 2021 | 0.40% | 0.40% | 1.25% | 1.25% | 1.25% | 1.25% | 1.25% | 1.25% |
|-----|-----|-----|-----|-----|-----|-----|-----|-----|
## Additional Ratios
# Year: Net Profit Margin / Return on Equity
|-----|-----|-----|-----|-----|-----|-----|-----|-----|
| 2014 | 0.40% | 0.40% | 1.25% | 1.25% | 1.25% | 1.25% | 1.25% | 1.25% |
| 2015 | 0.40% | 0.40% | 1.25% | 1.25% | 1.25% | 1.25% | 1.25% | 1.25% |
| 2016 | 0.40% | 0.40% | 1.25% | 1.25% | 1.25% | 1.25% | 1.25% | 1.25% |
| 2017 | 0.40% | 0.40% | 1.25% | 1.25% | 1.25% | 1.25% | 1.25% | 1.25% |
| 2018 | 0.40% | 0.40% | 1.25% | 1.25% | 1.25% | 1.25% | 1.25% | 1.25% |
| 2019 | 0.40% | 0.40% | 1.25% | 1.25% | 1.25% | 1.25% | 1.25% | 1.25% |
| 2020 | 0.40% | 0.40% | 1.25% | 1.25% | 1.25% | 1.25% | 1.25% | 1.25% |
| 2021 | 0.40% | 0.40% | 1.25% | 1.25% | 1.25% | 1.25% | 1.25% | 1.25% |
|-----|-----|-----|-----|-----|-----|-----|-----|-----|
## Activity Ratios
# Year: Inventory Turnover
|-----|-----|-----|-----|-----|-----|-----|-----|-----|
| 2014 | 7.84 | 7.84 | 1.25 | 1.25 | 1.25 | 1.25 | 1.25 | 1.25 |
| 2015 | 7.84 | 7.84 | 1.25 | 1.25 | 1.25 | 1.25 | 1.25 | 1.25 |
| 2016 | 7.84 | 7.84 | 1.25 | 1.25 | 1.25 | 1.25 | 1.25 | 1.25 |
| 2017 | 7.84 | 7.84 | 1.25 | 1.25 | 1.25 | 1.25 | 1.25 | 1.25 |
| 2018 | 7.84 | 7.84 | 1.25 | 1.25 | 1.25 | 1.25 | 1.25 | 1.25 |
| 2019 | 7.84 | 7.84 | 1.25 | 1.25 | 1.25 | 1.25 | 1.25 | 1.25 |
| 2020 | 7.84 | 7.84 | 1.25 | 1.25 | 1.25 | 1.25 | 1.25 | 1.25 |
| 2021 | 7.84 | 7.84 | 1.25 | 1.25 | 1.25 | 1.25 | 1.25 | 1.25 |
|-----|-----|-----|-----|-----|-----|-----|-----|-----|

```

Instruction

识别这篇作文的内容

识别到的小孩，他会堆雪人。他的手机丢了，留给我自己。少做傻事情哈。其实聪明人也可以很听话的，至少在没有长大以前，间你能不能不跟到你爸爸去。北京也一样吧。多穿衣服，多喝热水好了，我们就到这。以后再遇到吧。好久不见。很好吗？我很好！

② 六年级二班 - 王乐乐

Figure 9: Diverse OCR visualization. Kimi-VL demonstrates strong OCR capabilities across varied content types, including structured financial tables, complex mathematical formulas, and handwritten Chinese text. The model accurately parses tabular data into markdown, converts formulas to LaTeX, and transcribes handwritten paragraphs with contextual understanding, showcasing its versatility in multimodal text extraction and interpretation.

VL-7B (58.6%) and even Gemma-3-12B-IT (59.6%), despite having significantly fewer activated parameters. On video college-level problems, it significantly outperforms Qwen2.5-VL-7B and DeepSeek-VL2, only behind >10B Gemma-3-12B-IT, demonstrating reasonable university-level understanding capabilities compared to larger models. These results indicate that Kimi-VL effectively balances parameter efficiency with academic reasoning abilities.

4.1.2 General Visual Ability

Kimi-VL exhibits strong general visual understanding capabilities across multiple benchmarks. On MMBench-EN-v1.1, it achieves 83.1% accuracy, outperforming all efficient VLMs in comparison, and performing on par with GPT-4o. For AI2D, our model achieves 84.9% and surpasses all compared models including GPT-4o (84.6%). On MMVet, Kimi-VL scores 66.7% and ties closely with Qwen2.5-VL-7B (67.1%) and GPT-4o-mini (66.9%). For RealWorldQA, it achieves 68.1%, outperforming Gemma3-12B (59.1%) and approaching Qwen2.5-VL-7B (68.5%). These results demonstrate that our model maintains robust general visual understanding despite its compact architecture.

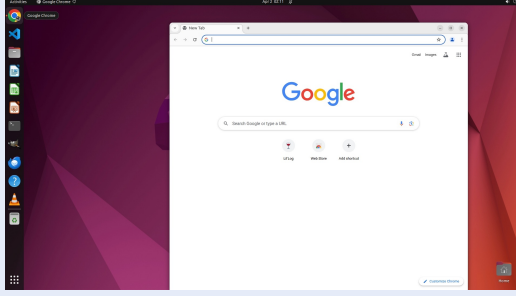
In multi-image reasoning tasks, Kimi-VL shows promising capabilities with a score of 57.3% on the BLINK benchmark. This performance surpasses Qwen2.5-VL-7B (56.4%), GPT-4o-mini (53.6%), Gemma3-12B-IT (50.3%), and Llama3.2-11B-Inst. (39.8%). The ability to reason across multiple images requires understanding spatial and temporal relationships between visual elements, which our model handles effectively with fewer parameters than most competitors.

4.1.3 Mathematical Reasoning

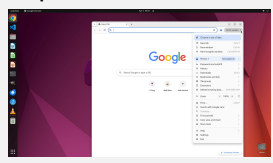
With its relatively small scale, Kimi-VL also demonstrates strong mathematical reasoning capabilities, particularly on the MathVista benchmark where it achieves 68.7%, outperforming all compared models including GPT-4o (63.8%) and Qwen2.5-VL-7B (68.2%). It indicates our model’s exceptional ability to understand and solve mathematical problems presented in visual contexts. On the more challenging MathVision benchmark, due to limited activated parameters,

 **Instruction:**

Can you enable the 'Do Not Track' feature in Chrome to enhance my online privacy?



Step 1

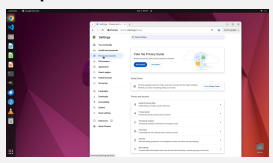


Thought: ... To enable the 'Do Not Track' feature, I need to access Chrome's settings. Looking at the interface, I can see the vertical ellipsis menu button in the top-right corner of the browser window. This menu button is the standard way to access Chrome's settings and other features. ...

Action: Click on the vertical ellipsis menu button in the top-right corner of the Chrome window to open the browser menu.

Toolcall: click(x=0.884, y=0.144)

Step 7

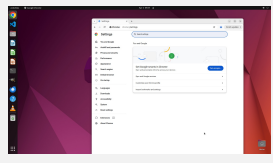


Thought: ... I notice that we're currently on the "Manage certificates" page, which is not where the "Do Not Track" setting would be located. ... To enable the "Do Not Track" feature, we need to navigate to the appropriate settings section. ...

Action: Click on the "Privacy and security" option in the left sidebar menu to expand its submenu.

Toolcall: click(x=0.365, y=0.317)

Step 2

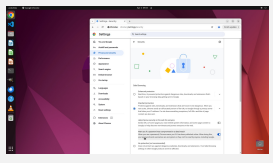


Thought: ... The next logical step would be to access Chrome's settings, where privacy options like "Do Not Track" are typically located. Looking at the menu that's currently open, I can see the "Settings" option at the bottom of the menu. This would be the most direct path to access privacy settings. ...

Action: Click on the "Settings" option in the Chrome menu to access the browser's settings page.

Toolcall: click(x=0.744, y=0.851)

Step 8

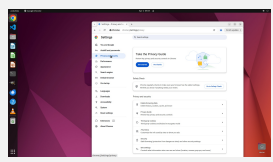


Thought: ... I can see that "Security" is one of the options in the Privacy and security section. This makes sense as "Do Not Track" is a security feature that helps protect user privacy by preventing websites from tracking browsing activity. ...

Action: Click on the "Security" option in the Privacy and security section to access more detailed security settings.

Toolcall: click(x=0.522, y=0.884)

Step 3

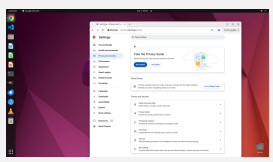


Thought: ... Now, I need to find where the "Do Not Track" setting is located. Based on my knowledge of Chrome's settings, this feature is typically found in the Privacy and security section. I can see that "Privacy and security" is one of the options in the left sidebar menu. ...

Action: Click on the "Privacy and security" option in the left sidebar menu.

Toolcall: click(x=0.386, y=0.311)

Step 9

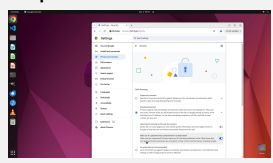


Thought: ... Since the current page doesn't show the "Do Not Track" setting, the logical next action would be to continue navigating through the settings. The back button in the browser would allow the user to return to the previous page and continue their search for the "Do Not Track" setting. ...

Action: Click the back button in the browser to return to the previous page.

Toolcall: click(x=0.486, y=0.242)

Step 4

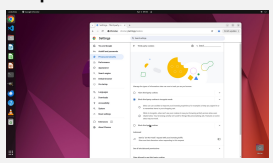


Thought: ... Now we need to find the "Do Not Track" setting. Looking at the current screen, I can see that "Do Not Track" is not immediately visible in the list of options. However, I notice that there's a "Security" option with a lock icon that might contain privacy-related settings including "Do Not Track". ...

Action: Click on the "Security" option in the Privacy and security section to access more detailed security settings.

Toolcall: click(x=0.522, y=0.884)

Step 10

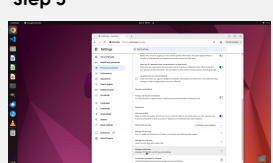


Thought: ... Looking at the available options, "Third-party cookies" is visible in the list. This option controls whether third-party cookies are blocked in Incognito mode. While this isn't exactly "Do Not Track," it is related to privacy controls. ...

Action: Click on the "Third-party cookies" option in the Privacy and security section to access its settings.

Toolcall: click(x=0.542, y=0.772)

Step 5

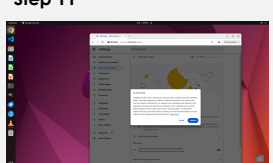


Thought: ... To find the "Do Not Track" setting, I need to scroll down in the Security section. The current view doesn't show all available options, and the "Do Not Track" setting is likely further down the page. Scrolling down will reveal more settings options that aren't currently visible. ...

Action: Scroll down in the Security settings page to reveal more options.

Toolcall: scroll(-5)

Step 11



Thought: ... I notice there's an "Advanced" section in the current view that contains a "Send a 'Do Not Track' request with your browsing traffic" option. This is exactly what we need to enable the "Do Not Track" feature. The toggle switch for this option is currently off. ...

Action: Click the toggle switch next to "Send a 'Do Not Track' request with your browsing traffic" to enable the feature.

Toolcall: click(x=0.808, y=0.871)

Step 6



Thought: ... The "Manage HTTPS/SSL certificates and settings" option is visible in the list. This is likely where the "Do Not Track" setting would be located, as certificate management is related to privacy and security features. ...

Action: Click on the "Manage HTTPS/SSL certificates and settings" option to access certificate management settings.

Toolcall: click(x=0.527, y=0.883)

Step 12



Thought: ... The dialog explains what "Do Not Track" does and has two buttons: "Cancel" and "Confirm". To complete the task of enabling this feature, we need to confirm the action by clicking the "Confirm" button. ...

Action: Click the "Confirm" button to enable the "Do Not Track" feature.

Toolcall: click(x=0.708, y=0.669)

Figure 10: Kimi-VL is capable of following multi-step reasoning processes to complete complex GUI tasks. In this example, it successfully enables the "Do Not Track" feature in the Chrome browser to enhance online privacy. The agent interprets each screen, identifies relevant UI elements, and performs the appropriate actions sequentially with clear thoughts, actions, and API calls.

Instruction

Please split this video into scenes, providing start time, end time, and detailed descriptions for each scene.



Response

(00:00:00 - 00:00:15) The scene opens with a close-up of an elderly person's face, highlighting their furrowed brow and weathered skin. The atmosphere is mysterious and intriguing, with the dim lighting and the steam rising from the coffee pot creating a sense of anticipation. At 00:00:05, text appears on the screen, reading 'THIS NORTH FACE PRESENTS', which serves as the title for the theme of the video. The person continues to cook, and at 00:00:13, the scene briefly transitions to a black screen with glowing particles before the next segment. The overall mood is mysterious and intimate, aligning with the theme of the video.

(00:00:16 - 00:00:24) The scene opens with a close-up of an elderly person's face, highlighting their furrowed brow and weathered skin. The atmosphere suggests a life of hardship and resilience (00:00:15 - 00:00:20). The camera then shifts to their yellow jacket, highlighting the texture and details, and a prayer wheel comes into view, held by the person (00:00:20 - 00:00:27). The focus then moves to the prayer wheel, capturing its intricate details and the serene expression of the elderly person as they spin it (00:00:27 - 00:00:32). The atmosphere is calm and contemplative, with the dim lighting and the sound of spinning prayer wheels creating a sense of spiritual reflection. The scene introduces a sense of cultural and spiritual depth, emphasizing themes of contemplation, spirituality, and the passage of time.

(00:00:33 - 00:00:46) The scene opens with a breathtaking aerial view of majestic snow-capped mountains, setting the stage for a theme of natural grandeur and adventure. The camera captures the serene and awe-inspiring landscape, which transitions to a title card at 00:00:38, introducing the film as 'A NEW FILM BY SHERPAS CINEMA'. The title card remains on screen until 00:00:45, after which the camera continues to showcase the stunning mountain range. The scene then shifts to a close-up of a person's eye at 00:00:46, subtly hinting at the personal stories and human elements that will unfold within this vast and beautiful setting. The overall mood is one of awe and inspiration, emphasizing the scale and beauty of the natural world.

(00:00:47 - 00:01:00) The scene opens with a close-up of a person's eye, with a camera shift to a detailed shot of a yellow jacket, emphasizing the texture and craftsmanship. The scene then moves to a close-up of a person's hands holding a prayer wheel, with the camera focusing on the intricate designs and the serene expression of the elderly person as they spin it (00:00:54 - 00:01:00). Following this, the scene moves to an underwater view, showcasing the serene and mysterious environment beneath the surface (00:01:00 - 00:01:03). The camera then pans to a majestic mountain range, highlighting the grandeur and scale of the natural world (00:01:03 - 00:01:09). The mood throughout the scene is one of awe and tranquility, blending elements of nature, spirituality, and the profound connection between the individual and the vastness of the world around them.

(00:01:10 - 00:01:27) The scene opens with an interior shot of a room filled with numerous candles arranged on a table, creating a serene and contemplative atmosphere. The camera then transitions to a close-up of an elderly person's face, their furrowed brow and weathered skin hinting at a life of experience and wisdom. The focus shifts to the intricate details of their yellow jacket, emphasizing the texture and craftsmanship. The scene then moves to a close-up of a person's hands holding a prayer wheel, with the camera focusing on the intricate designs and the serene expression of the elderly person as they spin it, before panning out to reveal the majestic mountain range in the background. The scene then cuts to a close-up of a rock surface, its rugged texture and natural patterns standing in contrast to the previous serene and spiritual elements. The camera then shifts to a view of clouds and treeline, with the mountain peaks peeking through, before moving to a close-up of snow-covered branches. The scene concludes with a wide shot of the natural environment. The scene then transitions to an aerial shot of a river, its winding path cutting through the landscape, before finally focusing on a close-up of a hand holding a prayer wheel. Throughout the scene, the themes of spirituality, tradition, and the beauty of nature are woven together, creating a sense of awe and reflection.

(00:01:28 - 00:01:39) The scene opens with a close-up of a person wearing a yellow jacket, focusing on the intricate details of their clothing, which suggests a sense of preparation and readiness. At 00:01:29, the camera shifts to a close-up of an eye, capturing the intensity and focus of the individual. The scene then transitions to an aerial view of a breathtaking snow-covered mountain range at 00:01:34, emphasizing the vastness and grandeur of the landscape. The camera slowly pans across the mountains, highlighting their rugged beauty and the serene, untouched nature of the environment. The overall mood of the scene is one of anticipation and awe, as the viewer is introduced to the challenging and majestic setting that lies ahead. The theme of preparation and the awe-inspiring nature of the landscape are prominently featured, setting the stage for what is to come.

(00:01:40 - 00:02:03) The scene opens with a group of climbers ascending a steep, snow-covered mountain, their movements slow and deliberate as they navigate the treacherous terrain (00:01:40 - 00:01:44). The camera then shifts to a close-up of a hand holding a piece of a book, showing a close-up of the pages providing instructions for safety (00:01:44 - 00:01:50). Next, the scene transitions to a wide view of a snow-covered mountain range, with the camera panning across the landscape to emphasize the scale and beauty of the environment (00:01:50 - 00:01:56). A skier is then shown descending a steep, snowy slope, the camera following their swift and agile movements as they carve through the powder (00:01:56 - 00:02:03). The sequence concludes with a close-up of a snow-covered mountain ridge, the pristine white landscape highlighting the raw power and majesty of nature (00:02:03). Throughout the scene, the theme of human determination and the awe-inspiring beauty of nature is prominently featured, capturing the essence of adventure and the challenge of conquering the elements.

(00:02:04 - 00:02:17) The scene opens with a close-up of a prayer wheel, its intricate details highlighted by the soft, diffused lighting. At 00:02:03, the camera then transitions to a breathtaking view of a snow-capped mountain peak, emphasizing the grandeur and majesty of the natural world. The serene and contemplative mood is maintained as the scene shifts to a close-up of a vintage watch at 00:02:05, its hands frozen in time. This is followed by a shot of a person in a tent, illuminated by a warm, yellow light, suggesting a moment of quiet reflection or preparation. At 00:02:08, the scene cuts to a climber's harness, with carabiners attached, symbolizing readiness and the technical aspects of the climb. The tension builds as two climbers are shown on a snowy ridge at 00:02:09, their silhouettes stark against the bright snow. The climax of the scene is reached at 00:02:12, with a skier launching off a cliff. The camera capturing the burst of snow and the skier's descent, requires a shot of a shot, where the camera follows the skier's path through the air, highlighting the skill and the dynamic, exhilarating nature of the sport, while also highlighting the inherent dangers and the thrill of the adventure. The editing effectively weaves together themes of preparation, reflection, and the intense, awe-inspiring moments of a mountain climb.

(00:02:18 - 00:02:42) The scene opens with a skier performing a mid-air trick, showcasing their skill and agility against the backdrop of a snowy mountain slope (00:02:17 - 00:02:20). The camera then transitions to a skier in a blue jacket, who is captured mid-air as they soar through a cloud of snow, emphasizing the dynamic and thrilling nature of the sport (00:02:20 - 00:02:23). The focus shifts to a skier in a red helmet, who is seen navigating through a dense forest of snow-covered trees, highlighting the technical aspects of the descent (00:02:23 - 00:02:26). The action intensifies with a skier in a red jacket, who is shown launching off a cliff and then landing smoothly on a slope, demonstrating precision and control. The scene then shifts to a skier performing a mid-air trick in a snowy landscape (00:02:26 - 00:02:29), with the skier launching off a cliff. The camera then follows the skier's path through the air, highlighting the skill and the dynamic, exhilarating nature of the sport, while also highlighting the inherent dangers and the thrill of the adventure. The editing effectively weaves together themes of preparation, reflection, and the intense, awe-inspiring moments of a mountain climb.

(00:02:43 - 00:03:05) The scene opens with a skier performing a mid-air trick against a stunning sunset backdrop, capturing the thrill and freedom of the sport (00:02:42 - 00:02:46). The camera then transitions to a skier that of incense burning, symbolizing a moment of reflection and spirituality (00:02:46 - 00:02:52). This is followed by a breathtaking view of a snow-covered mountain range under a pink sky, emphasizing the awe-inspiring beauty of nature (00:02:52 - 00:02:59). The scene then shifts to a skier riding a wave, highlighting the dynamic and exhilarating aspects of water sports (00:02:59 - 00:03:04). The overall mood of the scene is a blend of thrill, reflection, and the majesty of nature, with each shot seamlessly transitioning to the next, creating a cohesive and visually captivating sequence.

(00:03:06 - 00:03:27) The scene begins with a serene shot of a forest, where sunlight filters through the trees, creating a peaceful and introspective atmosphere. At 00:03:04, the camera shifts to a temple, where people are seen walking, adding a sense of cultural and spiritual depth to the setting. The temple is adorned with prayer flags, which flutter gently in the breeze, symbolizing hope and aspiration. At 00:03:08, the focus narrows to a close-up of prayer flags, their vibrant colors and intricate designs standing out against the backdrop of the temple. The scene then transitions to a forest floor covered in fallen leaves, evoking a sense of the change of seasons and the cycle of life. At 00:03:10, the camera captures the intricate textures of the fallen leaves, emphasizing the intricate details of the natural world. The scene then shifts to a wide shot of a rocky, reddish-brown landscape, with a person walking across it, their path leading towards the horizon under a clear blue sky, which adds a sense of vastness and isolation. At 00:03:11, the title 'INTO THE MIND' appears on the screen, setting the theme for the sequence. The camera then zooms in on the cracked earth, highlighting the textures and patterns of the ground, before fading to black at 00:03:15. The credits roll, listing the names of the cast and crew, and the scene concludes with a black screen at 00:03:27.

(00:03:28 - 00:03:37) The scene opens with a black screen displaying the credits, acknowledging the contributions of various individuals and organizations involved in the making of the film. The mood is neutral and informative, setting the stage for the conclusion of the narrative. As the credits roll, the screen transitions to a dark, rocky interior, likely a cave or a similar natural formation, with a wooden structure partially visible. This shift in setting suggests a change in the visual style, possibly indicating a new chapter or a different aspect of the story. The credits continue to display on the screen, providing a final overview of the production team and their roles. The scene then fades to black, marking the end of the film.

Figure 11: Video scene splitting. Kimi-VL processes a long-form video by segmenting it into coherent scenes and providing detailed start/end timestamps along with fine-grained natural language descriptions for each scene.[†]

Kimi-VL outperforms DeepSeek-VL2 and Llama-3.2-11B-Inst., but lags behind Qwen2.5-VL-7B and Gemma-12B-IT. Nevertheless, through RL and test-time scaling, Kimi-VL-Thinking has significantly improved and already on par with 30B-level VLMs (see Table 4). These results highlight our model’s effectiveness in combining visual perception with mathematical problem-solving, an essential capability for real-world applications.

4.1.4 Document Understanding and OCR

Kimi-VL excels in document understanding and OCR tasks across all benchmarks in this category. On InfoVQA, it achieves 83.2% accuracy, outperforming GPT-4o (80.7%) and DeepSeek-VL2 (78.1%). For OCRBench, our model scores 86.7%, surpassing all other models including GPT-4o-mini (78.5%) and DeepSeek-VL2 (81.1%). These results demonstrate that our model has exceptional text recognition and document understanding capabilities, making it especially suitable for applications involving document processing and information extraction.

[†]Video source: <https://vimeo.com/channels/top/54348266>

15

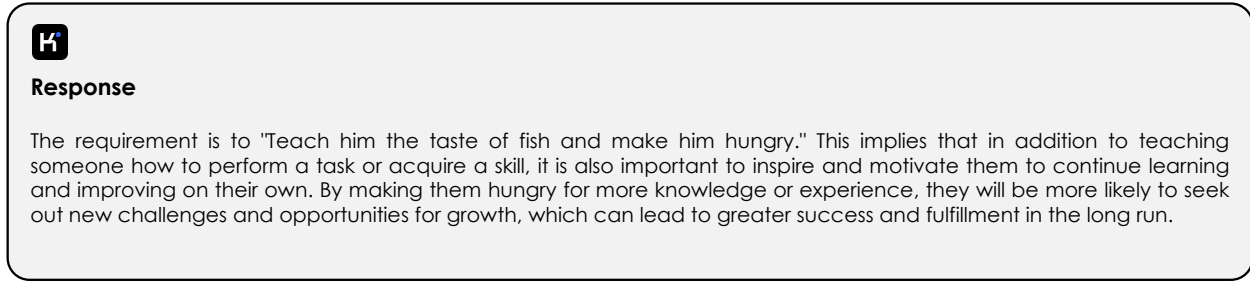
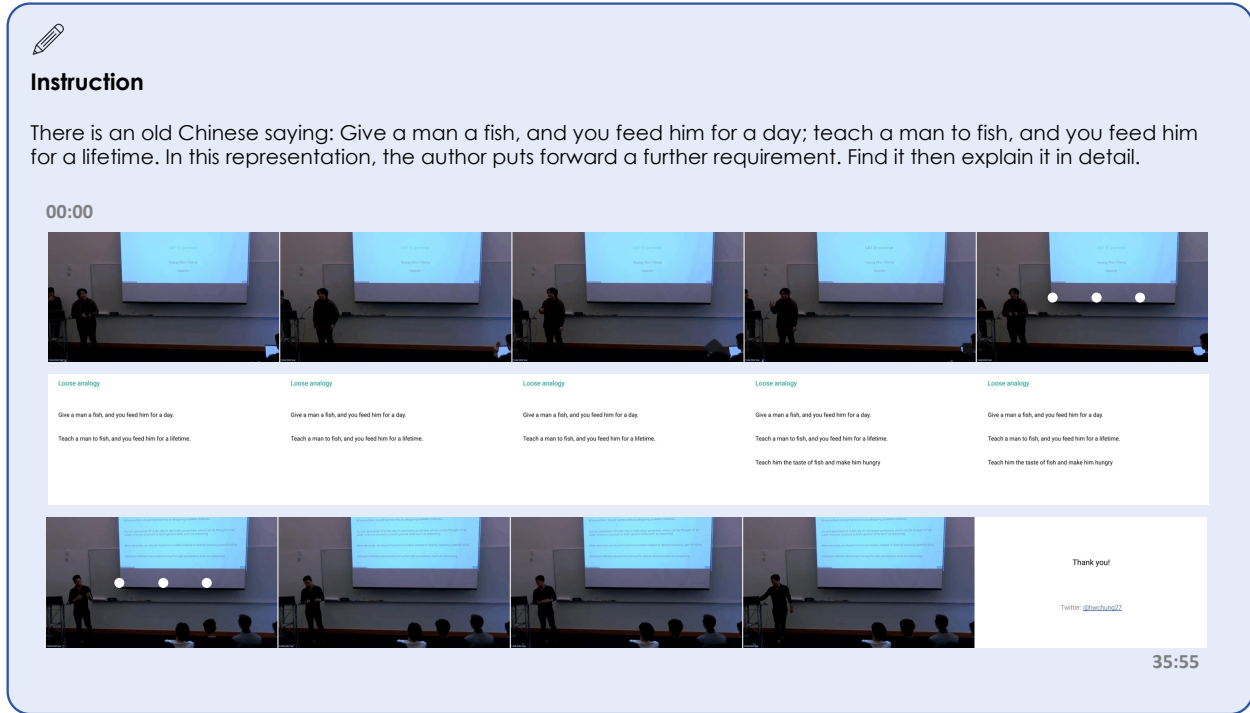


Figure 12: Catching and understanding key details from an hour-long video course. Kimi-VL demonstrates its ability to comprehend and interpret instructional video content by analyzing frame sequences and extracting conceptual progression over time. In this case, the model identifies a deepening of the traditional saying “Teach a man to fish, and you feed him for a lifetime” into a more nuanced idea: “Teach him the taste of fish and make him hungry.”[‡]

4.1.5 Agent Grounding and Multi-turn Agent Interaction

In agent-based tasks, Kimi-VL demonstrates remarkable performance. On single-step grounding, our model shows strong accuracy, with 92.0% on ScreenSpot-V2 and 34.5% on extremely difficult ScreenSpot-Pro (on 4K screens), proving its strong agent grounding abilities. More importantly, it also shows strong multi-step turn agent interaction abilities: For OSWorld, Kimi-VL reaches 8.22%, outperforming GPT-4o (5.03%) and other capable open-source models; On WindowsAgentArena, our model achieves 10.4%, also surpassing GPT-4o (9.4%) and others. These results highlight Kimi-VL’s exceptional ability to understand and interact with operating system interfaces, suggesting strong potential for applications in automated UI navigation and task execution.

4.1.6 Long Document and Long Video Understanding

Kimi-VL demonstrates competitive performance in long-form content understanding. On MMLongBench-Doc, a challenging benchmark with question-answering on up to 100+ pages, it achieves 34.7%, outperforming GPT-4o-mini (29.0%) and Qwen2.5-VL-7B (29.6%), only behind GPT-4o (42.8%). For long video understanding, on Video-MME, our model outperforms all efficient VLMs and especially leads on the fairer *w/o subtitle* setting, where models have to find answers from video frames instead of hacking from input subtitles; on *w/ subtitle* setting, it also reaches

[‡]Video source: https://www.youtube.com/watch?v=kYWUEV_e2ss

Benchmark (Metric)	Non-Thinking Model						Thinking Model			
	GPT-4o	GPT-4o-mini	Qwen2.5-VL-72B	Gemma-3-7B	Gemma-3-27B	Gemma-3-12B	o1-1217	QVQ-72B-Preview	Kimi-k1.5	Kimi-VL-Thinking-A3B
MathVision (full) (Pass@1)	30.4	-	38.1	25.1	35.5	32.1	-	35.9	38.6	36.8
MathVista (mini) (Pass@1)	63.8	56.7	74.8	68.2	62.3	56.4	71.0	71.4	74.9	71.3
MMMU (val) (Pass@1)	69.1	60.0	74.8	58.6	64.8	59.6	77.3	70.3	70.0	61.7

Table 4: Performance of the Kimi-VL-Thinking against various open-source and proprietary models across different benchmarks. The metrics evaluated include MathVista (mini), MMMU (val), and MathVision (full), with results expressed in terms of Pass@1. The Kimi-VL-Thinking outperforms the non-thinking models in most cases, showcasing the enhanced reasoning and processing capabilities of the “thinking” variant across different domains and scales.

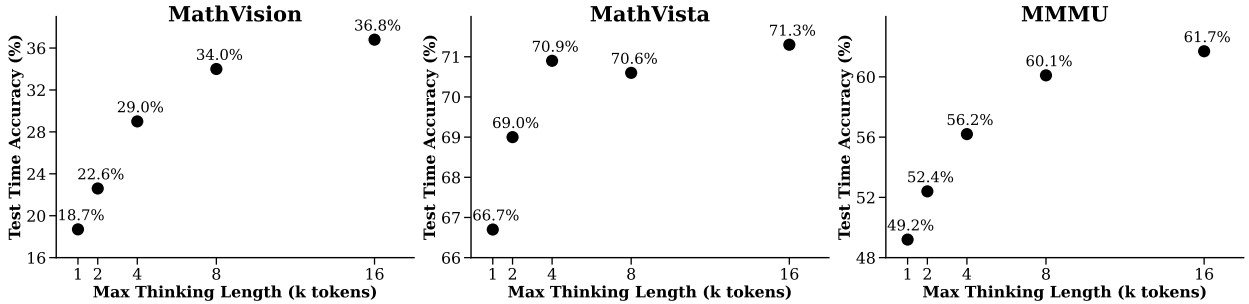


Figure 13: Test-time accuracy when scaling the max thinking token length of our **Kimi-VL-Thinking** model.

extraordinary 72.6% accuracy. On the MCQ subset of MLVU, Kimi-VL achieves an impressive 74.2% score, achieving state-of-the-art and surpassing both GPT-4o (64.6%) and Qwen2.5-VL-7B (70.2%). For LongVideoBench, it scores 64.5%, outperforming all compared models except GPT-4o (66.7%). These results demonstrate Kimi-VL’s strong capability to understand long-form PDFs and videos.

4.1.7 Egocentric and Fine-grained Video Perception

Kimi-VL also shows strong performance in more nuanced video perception tasks. On EgoSchema full set (*hidden test set*), it achieves 78.5%, significantly outperforming GPT-4o (72.2%), Qwen2.5-VL-7B (65.0%). For VSI-Bench, a very challenging benchmark that requires to understand spatial relationships and correspondences of multiple objects in a video, our model scores 37.4%, surpassing GPT-4o (34.0%) and Qwen2.5-VL-7B (34.2%). In TOMATO that examines fine-grained temporal perception of VLMs, Kimi-VL reaches 31.7%, outperforming Qwen2.5-VL-7B (27.6%) and GPT-4o-Mini (28.8%). These results demonstrate our model’s strong capability to understand dynamic visual content, track objects over time, and interpret complex actions in video sequences, making it well-suited for applications requiring temporal visual understanding.

4.2 A Reasoning Extension of Kimi-VL

Furthermore, we conduct a reasoning extension to empower Kimi-VL to reason with CoT and present a long-thinking version of the model, **Kimi-VL-Thinking**, through long-CoT activation and reinforcement learning. We validate its superior performance on several image benchmarks, as shown in Table 4.

Kimi-VL-Thinking significantly improves over the base Kimi-VL model, with gains of 2.6% on MathVista, 4.7% on MMMU, and 15.4% on MathVision, demonstrating its capability to leverage test-time computation for deeper reasoning and better handling of complex multimodal queries. In Table 4, Kimi-VL-Thinking further outperforms or rivals state-of-the-art thinking and non-thinking models: achieving 71.3% on MathVista, outperforming GPT-4o (63.8%) and GPT-4o-mini (56.7%); scoring 61.7% on MMMU, surpassing GPT-4o-mini (60.0%) and Qwen2.5-VL-7B (58.6%); and reaching 36.8% on MathVision, exceeding GPT-4o (30.4%) and Gemma-3-27B-IT (35.5%), even QVQ-72B (35.9%). While marginally behind some larger-scale models on select benchmarks, Kimi-VL-Thinking accomplishes these results with only 3B activated parameters—orders of magnitude fewer than its counterparts—underscoring its strong efficiency and effectiveness in multimodal reasoning.

Our Kimi-VL-Thinking model also exhibits strong test-time scaling properties, as shown in Figure 13. Specifically, increasing the max thinking token length at inference time consistently improves test-time accuracy across all three benchmarks. For example, on **MathVision**, the accuracy rises steadily from 18.7% at 1k tokens to 36.8% at 16k tokens, and similar upward trend is also observed on **MMMU**, indicating that the model is able to utilize longer reasoning chains for better performance. However, not all benchmarks benefit equally from longer thinking lengths. On **MathVista**, performance saturates early, with accuracy reaching 70.9% at 4k tokens and no further significant gains observed as the token length increases to 16k. It suggests that for this task, the necessary reasoning depth is already captured within a relatively short context, and additional computation does not yield further improvements.

5 Conclusion, Limitation, and Future Work

We introduce Kimi-VL, a VLM designed with a balanced approach to cover both multimodal and text-only pre-training/post-training, underpinned by an MoE-based architecture for scalable efficiency. Its 128K extended context window enables precise retrieval in lengthy texts and videos, while the native-resolution encoder MoonViT helps maintain high accuracy with low computational overhead in ultra-high-resolution visual tasks. Additionally, Kimi-VL-Thinking facilitates effective long-chain reasoning in complex image and video inference. Overall, Kimi-VL demonstrates robust adaptability and efficiency across multimodal, long-context, and high-resolution tasks, indicating substantial potential for future research and industrial applications.

However, Kimi-VL still faces several challenges:

1. Although the current model size performs effectively for many standard tasks, it remains too limited to address highly specialized or domain-specific problems, or problems that are strongly dependent on language abilities, restricting Kimi-VL’s ability to handle extremely complex scenarios.
2. While the reasoning capability is already strong for typical use cases, it has yet to reach its theoretical upper bound, particularly for intricate tasks requiring multi-step inference or deeper contextual understanding.
3. Despite providing a 128K extended context window, due to limited parameters in its attention layers (which is only comparable to a 3B model), its long-context abilities is still insufficient for certain advanced applications that involve extremely long sequences or high-volume contextual information.

In the future, we will tackle these challenges by scaling up the model size, expanding pre-training data, and enhancing post-training algorithms. Our next steps include optimizing Kimi-VL and releasing larger versions, as well as refining post-training and test-time scaling mechanisms for a better thinking model. These efforts will pave the way for more advanced applications in both research and industry.

template

- Amazon Web Services. *Amazon Simple Storage Service (Amazon S3)*. Web. Available at: <https://aws.amazon.com/s3/>. 2023. URL: <https://aws.amazon.com/s3/> (visited on 12/15/2023).
- Bai, Shuai et al. *Qwen2.5-VL Technical Report*. 2025. arXiv: 2502.13923 [cs.CV]. URL: <https://arxiv.org/abs/2502.13923>.
- Bonatti, Rogerio et al. *Windows Agent Arena: Evaluating Multi-Modal OS Agents at Scale*. 2024. arXiv: 2409.08264 [cs.AI]. URL: <https://arxiv.org/abs/2409.08264>.
- Chen, Lin et al. “Are We on the Right Way for Evaluating Large Vision-Language Models?” In: *arXiv preprint arXiv:2403.20330* (2024).
- Chen, Tianqi et al. *Training Deep Nets with Sublinear Memory Cost*. 2016. arXiv: 1604.06174 [cs.LG]. URL: <https://arxiv.org/abs/1604.06174>.
- Cheng, Kanzhi et al. “Seeclick: Harnessing gui grounding for advanced visual gui agents”. In: *arXiv preprint arXiv:2401.10935* (2024).
- Dao, Tri et al. *FlashAttention: Fast and Memory-Efficient Exact Attention with IO-Awareness*. 2022. arXiv: 2205.14135 [cs.LG]. URL: <https://arxiv.org/abs/2205.14135>.
- DeepSeek-AI, Daya Guo, et al. *DeepSeek-R1: Incentivizing Reasoning Capability in LLMs via Reinforcement Learning*. 2025. arXiv: 2501.12948 [cs.CL]. URL: <https://arxiv.org/abs/2501.12948>.
- DeepSeek-AI, Aixin Liu, et al. *DeepSeek-V3 Technical Report*. 2025. arXiv: 2412.19437 [cs.CL]. URL: <https://arxiv.org/abs/2412.19437>.
- Dehghani, Mostafa et al. *Patch n’ Pack: NaViT, a Vision Transformer for any Aspect Ratio and Resolution*. 2023. arXiv: 2307.06304 [cs.CV]. URL: <https://arxiv.org/abs/2307.06304>.

- Fedus, William, Barret Zoph, and Noam Shazeer. *Switch Transformers: Scaling to Trillion Parameter Models with Simple and Efficient Sparsity*. 2022. arXiv: 2101.03961 [cs.LG]. URL: <https://arxiv.org/abs/2101.03961>.
- Fu, Chaoyou et al. “Video-MME: The First-Ever Comprehensive Evaluation Benchmark of Multi-modal LLMs in Video Analysis”. In: *arXiv:2405.21075* (2024).
- Fu, Xingyu et al. “Blink: Multimodal large language models can see but not perceive”. In: *European Conference on Computer Vision*. Springer, 2024, pp. 148–166.
- Gadre, Samir Yitzhak et al. “Datacomp: In search of the next generation of multimodal datasets”. In: *Advances in Neural Information Processing Systems 36* (2024).
- Grauman, Kristen et al. “Ego4d: Around the world in 3,000 hours of egocentric video”. In: *Proceedings of the IEEE/CVF conference on computer vision and pattern recognition*. 2022, pp. 18995–19012.
- Guo, Jarvis et al. *MAmmoTH-VL: Eliciting Multimodal Reasoning with Instruction Tuning at Scale*. 2024. arXiv: 2412.05237 [cs.CL]. URL: <https://arxiv.org/abs/2412.05237>.
- Hu, Kairui et al. “Video-MMMU: Evaluating Knowledge Acquisition from Multi-Discipline Professional Videos”. In: *arXiv preprint arXiv:2501.13826* (2025).
- Huang, Yanping et al. *GPipe: Efficient Training of Giant Neural Networks using Pipeline Parallelism*. 2019. arXiv: 1811.06965 [cs.CV]. URL: <https://arxiv.org/abs/1811.06965>.
- Jacobs, Sam Ade et al. *DeepSpeed Ulysses: System Optimizations for Enabling Training of Extreme Long Sequence Transformer Models*. 2023. arXiv: 2309.14509 [cs.LG]. URL: <https://arxiv.org/abs/2309.14509>.
- Jordan, Keller et al. *Muon: An optimizer for hidden layers in neural networks*. 2024. URL: <https://kellerjordan.github.io/posts/muon/>.
- Kembhavi, Aniruddha et al. “A diagram is worth a dozen images”. In: *European conference on computer vision*. Springer, 2016, pp. 235–251.
- Korthikanti, Vijay et al. *Reducing Activation Recomputation in Large Transformer Models*. 2022. arXiv: 2205.05198 [cs.LG]. URL: <https://arxiv.org/abs/2205.05198>.
- Laurençon, Hugo et al. “Obelics: An open web-scale filtered dataset of interleaved image-text documents”. In: *Advances in Neural Information Processing Systems 36* (2024).
- Li, Bo et al. *LLaVA-OneVision: Easy Visual Task Transfer*. 2024. arXiv: 2408.03326 [cs.CV]. URL: <https://arxiv.org/abs/2408.03326>.
- Li, Dongxu et al. *Aria: An Open Multimodal Native Mixture-of-Experts Model*. 2024. arXiv: 2410.05993 [cs.CV]. URL: <https://arxiv.org/abs/2410.05993>.
- Li, Kaixin et al. “ScreenSpot-Pro: GUI Grounding for Professional High-Resolution Computer Use”. In: *Workshop on Reasoning and Planning for Large Language Models*. 2025.
- Li, Shen et al. *PyTorch Distributed: Experiences on Accelerating Data Parallel Training*. 2020. arXiv: 2006.15704 [cs.DC]. URL: <https://arxiv.org/abs/2006.15704>.
- Liu, Hao, Matei Zaharia, and Pieter Abbeel. *Ring Attention with Blockwise Transformers for Near-Infinite Context*. 2023. arXiv: 2310.01889 [cs.CL]. URL: <https://arxiv.org/abs/2310.01889>.
- Liu, Jingyuan et al. “Muon is Scalable for LLM Training”. In: *arXiv preprint arXiv:2502.16982* (2025). – “Muon is Scalable for LLM Training”. In: *arXiv preprint arXiv:2502.16982* (2025).
- Liu, Yuan et al. “MMBench: Is Your Multi-modal Model an All-around Player?” In: *arXiv:2307.06281* (2023).
- Liu, Yuliang et al. “On the hidden mystery of ocr in large multimodal models”. In: *arXiv e-prints* (2023), arXiv-2305.
- Lu, Pan et al. “Mathvista: Evaluating mathematical reasoning of foundation models in visual contexts”. In: *arXiv preprint arXiv:2310.02255* (2023).
- Mangalam, Karttikeya, Raiymbek Akshulakov, and Jitendra Malik. “Egoschema: A diagnostic benchmark for very long-form video language understanding”. In: *Advances in Neural Information Processing Systems 36* (2023), pp. 46212–46244.
- Mathew, Minesh et al. “Infographiccvqa”. In: *Proceedings of the IEEE/CVF Winter Conference on Applications of Computer Vision*. 2022, pp. 1697–1706.
- Narayanan, Deepak et al. *Efficient Large-Scale Language Model Training on GPU Clusters Using Megatron-LM*. 2021. arXiv: 2104.04473 [cs.CL]. URL: <https://arxiv.org/abs/2104.04473>.
- OpenAI. “Learning to reason with LLMs”. In: (2024). URL: <https://openai.com/index/learning-to-reason-with-l1ms/>.
- OpenAI et al. *GPT-4o System Card*. 2024. arXiv: 2410.21276 [cs.CL]. URL: <https://arxiv.org/abs/2410.21276>.
- Rajbhandari, Samyam et al. “Zero: Memory optimizations toward training trillion parameter models”. In: *SC20: International Conference for High Performance Computing, Networking, Storage and Analysis*. IEEE, 2020, pp. 1–16.
- Schuhmann, Christoph et al. “Laion-5b: An open large-scale dataset for training next generation image-text models”. In: *Advances in Neural Information Processing Systems 35* (2022), pp. 25278–25294.

- Shangguan, Ziyao et al. “TOMATO: Assessing Visual Temporal Reasoning Capabilities in Multimodal Foundation Models”. In: *International Conference on Learning Representations*. 2025. URL: <https://openreview.net/forum?id=fCi4o83Mfs>.
- Su, Dan et al. “Nemotron-CC: Transforming Common Crawl into a Refined Long-Horizon Pretraining Dataset”. In: *arXiv preprint arXiv:2412.02595* (2024).
- Su, Jianlin et al. *RoFormer: Enhanced Transformer with Rotary Position Embedding*. 2023. arXiv: 2104.09864 [cs.CL]. URL: <https://arxiv.org/abs/2104.09864>.
- Team, Gemini et al. *Gemini 1.5: Unlocking multimodal understanding across millions of tokens of context*. 2024. arXiv: 2403.05530 [cs.CL]. URL: <https://arxiv.org/abs/2403.05530>.
- Team, Gemma et al. *Gemma 3 Technical Report*. 2025. arXiv: 2503.19786 [cs.CL]. URL: <https://arxiv.org/abs/2503.19786>.
- Team, Kimi et al. “Kimi k1.5: Scaling reinforcement learning with llms”. In: *arXiv preprint arXiv:2501.12599* (2025).
- Tong, Shengbang et al. *Cambrian-1: A Fully Open, Vision-Centric Exploration of Multimodal LLMs*. 2024. arXiv: 2406.16860 [cs.CV]. URL: <https://arxiv.org/abs/2406.16860>.
- Wang, Ke et al. “Measuring multimodal mathematical reasoning with math-vision dataset”. In: *arXiv preprint arXiv:2402.14804* (2024).
- Wei, Haoran et al. “General OCR Theory: Towards OCR-2.0 via a Unified End-to-end Model”. In: *arXiv preprint arXiv:2409.01704* (2024).
- Wu, Haoning et al. “Longvideobench: A benchmark for long-context interleaved video-language understanding”. In: *Advances in Neural Information Processing Systems* 37 (2024), pp. 28828–28857.
- Wu, Zhiyong et al. “Os-atlas: A foundation action model for generalist gui agents”. In: *arXiv preprint arXiv:2410.23218* (2024).
- Wu, Zhiyu et al. *DeepSeek-VL2: Mixture-of-Experts Vision-Language Models for Advanced Multimodal Understanding*. 2024. arXiv: 2412.10302 [cs.CV]. URL: <https://arxiv.org/abs/2412.10302>.
- x.ai. “Grok-1.5 Vision Preview”. In: (2024). URL: <https://x.ai/news/grok-1.5v>.
- Xie, Tianbao et al. “Osworld: Benchmarking multimodal agents for open-ended tasks in real computer environments”. In: *Advances in Neural Information Processing Systems* 37 (2024), pp. 52040–52094.
- Yang, Jihan et al. “Thinking in space: How multimodal large language models see, remember, and recall spaces”. In: *arXiv preprint arXiv:2412.14171* (2024).
- Yu, Jiahui et al. *CoCa: Contrastive Captioners are Image-Text Foundation Models*. 2022. arXiv: 2205.01917 [cs.CV]. URL: <https://arxiv.org/abs/2205.01917>.
- Yu, Weihao et al. “Mm-vet: Evaluating large multimodal models for integrated capabilities”. In: *International conference on machine learning*. PMLR. 2024.
- Yue, Xiang, Yuansheng Ni, et al. “Mmmu: A massive multi-discipline multimodal understanding and reasoning benchmark for expert agi”. In: *Proceedings of the IEEE/CVF Conference on Computer Vision and Pattern Recognition*. 2024, pp. 9556–9567.
- Yue, Xiang, Xingwei Qu, et al. “Mammoth: Building math generalist models through hybrid instruction tuning”. In: *arXiv preprint arXiv:2309.05653* (2023).
- Zhai, Xiaohua et al. *Sigmoid Loss for Language Image Pre-Training*. 2023. arXiv: 2303.15343 [cs.CV]. URL: <https://arxiv.org/abs/2303.15343>.
- Zhao, Yilun et al. “MMVU: Measuring Expert-Level Multi-Discipline Video Understanding”. In: *arXiv preprint arXiv:2501.12380* (2025).
- Zhou, Junjie et al. “Mlvu: A comprehensive benchmark for multi-task long video understanding”. In: *arXiv preprint arXiv:2406.04264* (2024).
- Zhu, Wanrong et al. “Multimodal c4: An open, billion-scale corpus of images interleaved with text”. In: *Advances in Neural Information Processing Systems* 36 (2024).

Appendix

A Contributions

Core Contributors

Bohong Yin	Jiaming Li
Bowei Xing	Jianlin Su
Cheng Chen	Jianzhou Wang
Chu Wei	Jiaqi Deng [#]
Dehao Zhang	Jiezhong Qiu
Dongliang Wang	Jin Xie
Haoning Wu*	Jinhong Wang
Haotian Yao	Jingyuan Liu
Haoyu Lu*	Junjie Yan
Hao Yang	Kun Ouyang
Lin Sui	Liang Chen
Xinyuan Wang [#]	Longhui Yu
Xinyu Zhou	Mengfan Dong
Yang Li	Mengnan Dong
Y. Charles*	Nuo Xu
Yiping Bao	Pengyu Cheng
Yimin Chen	Qizheng Gu
Yuxin Wu	Runjie Zhou
Zaida Zhou	Shaowei Liu
Zhaowei Li	Sihan Cao
Zhiqi Huang	Tao Yu [#]
Zhilin Yang	Tianhui Song
Ziwei Chen	Tongtong Bai

Contributors

Angang Du	Weiran He
Bowen Qu	Wei Song
Bowen Wang [#]	Weixiao Huang
Chenlin Zhang	Weixin Xu
Chenzhuang Du	Xiaokun Yuan
Congcong Wang	Xingzhe Wu
Dikang Du	Xingcheng Yao
Enming Yuan	Xinxing Zu
Enzhe Lu	Yangyang Hu
Fang Li	Yan Zhong
Flood Sung	Yanru Chen
Guangda Wei	Yibo Miao
Guokun Lai	Yejie Wang
Han Zhu	Yibo Liu
Hao Ding	Yidao Qin
Hao Hu	Yiqin Wang
Hao Zhang	Yongsheng Kang
Heng Wang	Yuanxin Liu
Hongcheng Gao	Yulun Du
Huabin Zheng	Yuzhi Wang

* Project lead(s).

The University of Hong Kong, Moonshot.ai

The listing of authors is in alphabetical order based on their first names.

B Evaluation Details

B.1 Image Benchmark

MMMU (Yue, Ni, et al. 2024) encompasses a carefully curated collection of 11.5K multimodal questions sourced from college exams, quizzes, and textbooks. These questions span six major academic fields: Art & Design, Business, Science, Health & Medicine, Humanities & Social Science, and Tech & Engineering.

MBBench-EN-v1.1 (Yuan Liu et al. 2023) is a fine-grained benchmark that contains 2974 multiple-choice questions, covering 20 ability dimensions. It incorporate perception and reasoning as the top-level ability dimensions in its ability taxonomy, leading to different levels of evaluation in various ability dimensions.

MMStar (Lin Chen et al. 2024) is an elite vision-indispensable multimodal benchmark comprising 1,500 challenge samples meticulously selected by humans. It is designed to benchmark 6 core capabilities and 18 detailed axes, aiming to evaluate the multimodal capacities of LVLMs with a carefully balanced and purified selection of samples.

MMVet (W. Yu et al. 2024) is designed based on the insight that the intriguing ability to solve complicated tasks is often achieved by a generalist model being able to integrate different core vision-language capabilities. It defines 6 core VL capabilities and examines the 16 integrations of interest derived from the capability combination.

RealWorldQA (x.ai 2024) is a benchmark designed to evaluate the real-world spatial understanding capabilities of multimodal models. It assesses how well the models comprehend physical environments. The benchmark consists of over 700 images, each accompanied by a question and a verifiable answer, and these images are drawn from various real-world scenarios.

AI2D (Kembhavi et al. 2016) is a dataset of over 5000 grade school science diagrams with over 150000 rich annotations, their ground truth syntactic parses, and more than 15000 corresponding multiple choice questions.

MathVision (K. Wang et al. 2024) is a carefully curated collection of 3,040 high-quality mathematical problems with visual contexts that are sourced from real math competitions. It covers 16 distinct mathematical disciplines and is graded across 5 levels of difficulty. This dataset offers a comprehensive and diverse set of challenges, making it ideal for evaluating the mathematical reasoning abilities of LMMs.

MathVista (P. Lu et al. 2023) is a benchmark that integrates challenges from a variety of mathematical and visual tasks, demanding participants to exhibit fine-grained, deep visual understanding along with compositional reasoning to successfully complete the tasks.

BLINK (X. Fu et al. 2024) is a benchmark designed to evaluate multi-image visual cognition, encompassing tasks related to depth relationships, feature matching, digital forensics, and spatiotemporal reasoning. It features a diverse set of multi-image perceptual similarity tasks, validated through standardized protocols.

InfoVQA (Mathew et al. 2022) is a dataset specifically designed to assess models’ capabilities in interpreting and reasoning with complex infographics that integrate text, graphics, and visual elements. Model performance on this dataset is evaluated using the ANLS metric on the test set.

OCRBench (Yuliang Liu et al. 2023) evaluates the OCR capabilities of MLLMs across five tasks: text recognition, scene text VQA, document VQA, key information extraction, and handwritten math expression recognition. The benchmark is scored out of a maximum of 1000 points.

B.2 Video and Long Document Benchmark

VideoMMU (K. Hu et al. 2025) is a video benchmark designed to evaluate the college-level knowledge acquisition capabilities of large multimodal models. It consists of 300 expert-level videos and 900 human-annotated questions. The videos span six diverse academic disciplines: Art, Humanities, Medicine, Business, Science, and Engineering. The questions are structured to align with three cognitive stages: Perception, Comprehension, and Adaptation.

MMVU (Y. Zhao et al. 2025) is a video benchmark designed to evaluate the expert-level video understanding ability. The benchmark contains 3,000 expert-annotated questions over 1,529 videos, which span 27 subjects from four core disciplines: Science, Healthcare, Humanities & Social Sciences, and Engineering.

Video-MME (C. Fu et al. 2024) is a video benchmark that consists of 900 manually selected videos (totaling 254 hours length), and 2,700 QA pairs. The videos, varying in duration, are categorized into 30 fine-grained classes across six diverse domains: Knowledge, Film & Television, Sports Competition, Artistic Performance, Life Record, and Multilingual content. Evaluations are conducted under two different settings: with and without subtitles.

MLVU (J. Zhou et al. 2024) is designed to evaluate the model performance in comprehending long videos from multiple aspects. It consists of 1,730 videos along with 3,102 corresponding question-answer pairs (2,593 in dev set and 509 in test set). Videos of this benchmark are collected from multiple scenarios, including Sport, Ego-centric, Life Record, Tutorial, etc. The close-ended task set of MLVU comprises 7 different tasks: Action Order, Action Count, Topic Reasoning, Anomaly Recognition, Plot QA, Ego Reasoning, and Needle QA.

LongVideoBench (H. Wu et al. 2024) is a video question-answering benchmark designed to evaluate the long-form multimodal perception and relation capability of large multimodal models. The benchmark includes 3,763 web-collected videos spanning various lengths and themes, along with their corresponding subtitles. It includes 6,678 human-annotated multiple-choice questions, distributed across 17 fine-grained categories, which accesses different aspects of video-language understanding.

EgoSchema (Mangalam et al. 2023) is a video benchmark designed to evaluate the long-form video understanding capabilities within the ego-centric scenario. Derived from Ego4D (Grauman et al. 2022), the benchmark comprises over 5,031 multiple choice question-answer pairs spanning more than 250 hours real-world videos with a semi-automatic data pipeline.

VSI-Bench (Yang et al. 2024) is designed to evaluate the visual-spatial comprehensive capabilities of large multimodal models. It consists of over 5,000 question-answer pairs across around 290 real indoor-scene videos.

TOMATO (Shangguan et al. 2025) is a video benchmark comprises 1,484 human-annotated question-answer pairs and 1,417 videos. TOMATO focuses on evaluating the temporal reasoning capabilities of large multimodal models, including action counting, direction prediction, rotation analysis, shape & trend detection, velocity & frequency estimation, and visual cue interpretation.

B.3 Agent Benchmark

ScreenSpot V2 (Zhiyong Wu et al. 2024) is an enhanced version of the ScreenSpot (K. Cheng et al. 2024) benchmark, which focuses on evaluating the performance of GUI grounding models across multiple platforms, including web, desktop, and mobile interfaces. This updated version addresses several issues identified in the original ScreenSpot dataset, such as incorrect or ambiguous annotations, spelling mistakes, and mislabeled bounding boxes.

ScreenSpot Pro (K. Li et al. 2025) is a benchmark for evaluating GUI grounding in high-resolution, complex UI environments. It contains 1,581 real-world, high-resolution images and expert-annotated tasks from diverse professional domains. Including domain-specific interface conventions that challenge models to understand professional-grade interfaces beyond consumer applications.

OSWorld (T. Xie et al. 2024) is a pioneering scalable, real computer environment designed for multimodal agents, facilitating task setup, execution-based evaluation, and interactive learning across multiple operating systems, including Ubuntu, Windows, and macOS. It serves as a unified platform for evaluating open-ended computer tasks that involve arbitrary applications, addressing the limitations of existing benchmarks that often lack interactive environments or are confined to specific applications or domains.

WindowsAgentArena (Bonatti et al. 2024) is a benchmark designed to evaluate multimodal agents in realistic Windows environments. Built on the OSWorld framework, it allows agents to interact with a full range of applications and web tools. The benchmark is scalable and can complete evaluations in under 20 minutes on Azure. It offers insights into agent performance, highlighting the potential for future research in agent development and task automation.